A Proposal for a Three Detector Short-Baseline Neutrino Oscillation Program in the Fermilab Booster Neutrino Beam

Part II: LAr1-ND Conceptual Design

January 8, 2015

CONTENTS

I. INTRODUCTION

The Fermilab Short Baseline Neutrino program includes the construction of a Liquid Argon Near Detector, LAr1-ND, at 110 m from the Booster neutrino source in a new enclosure. Leveraging the advanced design work performed for LBNE and the very recent experience of the MicroBooNE detector construction, the LAr1-ND project has the potential to move forward quickly. As described in Part I, LAr1-ND serves as the near detector in a three LAr-TPC experiment capable of definitively addressing existing anomalies in neutrino physics and making precision measurements of high-Δm^2 neutrino oscillations through both appearance and disappearance searches.

Due to the high event rate of neutrino interactions at the near location, significant physics output can be achieved with a relatively short run of the LAr1-ND experiment. In addition to the physics program, LAr1-ND, following the MicroBooNE model, will have a development program serving as an engineering prototype for LAr-TPCs for long-baseline CP-violation searches in the future.

This Conceptual Design Report for the LAr1-ND detector is organized as follows. Section II briefly reviews the LAr1-ND stand alone physics program. A short introduction to the LAr1-ND detector design and dimensions is given in Section III. Section IV presents the TPC design, while the TPC electronics, DAQ and trigger systems are described in Section V. Section VI describes a UV laser-based field calibration system. Different options for the scintillation light collection system under consideration are described in Section VII. An external cosmic ray tagging system will complement the experiment, as reported in Section VIII.

II. PHYSICS OF LAR1-ND

While LAr1-ND, in conjunction with MicroBooNE and the ICARUS-T600, is a critical part of the oscillation physics program described in Part I, as a stand alone detector it enables a large number of relevant physics results. In this section we will discuss a sub-set of the physics measurements that can be performed with LAr1-ND. These include studies of a possible MiniBooNE-like low energy excess of electromagnetic events that does not depend on the distance.

A. MiniBooNE Low Energy Excess

Looking for the low energy excess observed by the MiniBooNE experiment [1] and characterizing its nature is the main physics goal of the MicroBooNE experiment [2]. This excess of electromagnetic events could be due to neutrino interactions with either a single-electron or single-photon in the final state. Observation of a low energy excess signal by MicroBooNE in the years leading up to the beginning of LAr1-ND data taking would immediately lead to the question of whether that excess is intrinsic to the beam or appears over the 470 m distance between source and detector.

LAr1-ND, at 110 m from the BNB target, can search for the same excess in a relatively short time. Here we estimate the significance with which LAr1-ND would observe *the same* MiniBooNE-like electromagnetic excess ina the ν_e candidate sample. The methods used to estimate signal predictions for LAr1-ND for the model described above follows those of a study performed by the MicroBooNE Collaboration [3]. Specifically, the excess of events observed from

MiniBooNE is scaled to the LAr1-ND predicted reconstructed rates. This is done accounting for the MiniBooNE reconstruction and particle identification efficiencies as reported in [4] to correct the raw excess event rates in MiniBooNE as a function of (E_{lep}, θ_{lep}), and subsequently using the Monte Carlo predicted 2D matrix $[E_\nu^{true}, E_{lep}]$ for charged current inclusive events on argon in order to properly correct for the cross-section dependence of Ar versus CH_2 and the flux ratio at LAr1-ND with respect to MiniBooNE. Because only the lepton energy and angle are available in MiniBooNE data, we investigate the excess in LAr1-ND as a function of the 'lepton candidate' energy (after accounting for shower energy smearing).

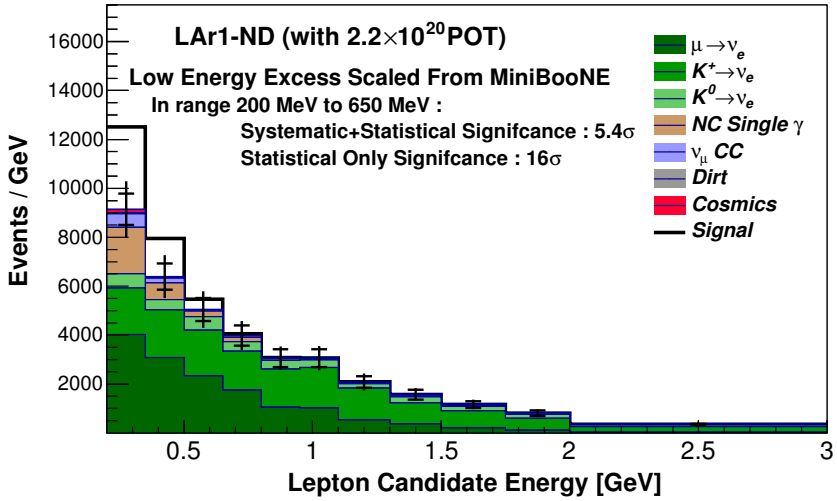

FIG. 1: *Scaled MiniBooNE low energy excess events as a function of the lepton candidate energy in LAr1-ND for an exposure of* 2.2×10^{20} *protons on target and using the same fiducial volume and backgrounds as the* ν_e *appearance analysis described in Part I of the proposal. The signal prediction assumes the effect observed by MiniBooNE is electrons but is* not distance dependent. *For the uncertainty on the background distribution the inner bars represent the statistical uncertainty and the outer bars represent the statistical + systematic uncertainties (see Part I).*

Using the ν_e charged current inclusive backgrounds and systematic uncertainties discussed in Part I, we quantify the significance of a MiniBooNE-like excess in LAr1-ND. In Fig. 1, we report the excess events stacked on top of the expected backgrounds. In the 200–650 MeV range in lepton energy, 803 excess events are expected, compared to a background of 3,177 events for an exposure of 2.2×10^{20} protons on target. This is a 5.4σ signal including both systematic and statistical uncertainties. Considering only statistical uncertainties, the excess sits $> 10\sigma$ above the background.

If MicroBooNE observes an excess of photons which are due to an as-yet unknown source of neutral current interactions producing single photons in the final state, LAr1-ND at 110 m will immediately confirm that the excess is intrinsic to the beam (i.e. that it is due to some un-modeled neutral current interaction). Also, the event rate with which LAr1-ND will be able to study these events will be more than one order of magnitude larger than MicroBooNE. Such a sample will enable a measurement of this reaction with great precision and inform the development of cross section models in this energy range to include this process.

B. Neutrino Cross Section Measurements

As discussed in Part I, neutrino-nucleus interactions are critical to understand in neutrino oscillation experiments, including the future liquid argon long-baseline program. LAr1-ND provides an ideal venue to conduct precision cross section measurements in the GeV energy range. The experiment will collect enormous neutrino event samples and, continuing the studies done by MicroBooNE and ICARUS, will make the world's highest statistics cross section measurements for many ν-Ar scattering processes.

Table I shows the expected rates of ν_μ and ν_e events separated into their main experimental topologies for an exposure of 6.6×10^{20} protons on target (POT). A novel approach based on the event categorization in terms of exclusive topologies can be used to analyze data and provide precise cross section measurements in many different ν_μ and ν_e exclusive channels. Included for reference, we also show the classification by physical process from Monte Carlo truth information.

The largest event sample corresponds to a ν_μ charged-current 0 pion final state, where there is an outgoing μ^-, one or more recoil nucleons, and no outgoing pions or kaons. This cross section for scattering off nuclei largely depends on final state interactions and other nuclear effects and LAr1-ND data will allow the study of nuclear effects in neutrino interactions in argon nuclei with high precision.

In LAr1-ND more than 2 million neutrino interactions will be collected per year in the full active volume (assuming 2.2×10^{20} POT), with 1.5 million ν_μ and 12,000 ν_e charged current (CC) events. One year exposure of LAr1-ND will provide an event sample 6-7 times larger than will be available in the full MicroBooNE phase I run.

Comparison of ν_e CC and ν_μ CC cross sections is very important. By lepton universality, the cross sections should be the same after correcting for the outgoing charged-lepton mass. A difference in the cross sections would indicate a new process that violates lepton universality.

LAr1-ND will also see several hundred $\nu_\mu e \to \nu_\mu e$ elastic scattering events in 6.6×10^{20} POT. These events are easily identified by an outgoing electron along the neutrino beam direction with $\cos\theta > 0.99$ and with no recoil nucleons. With this event sample, a measurement of $\sin^2\theta_W$ can be made at relatively low energy to be compared with the world average.

We expect approximately a quarter million NC elastic scattering events identified by a single nucleon (proton or neutron) recoil track. If the recoil proton events can be cleanly separated from the recoil neutron events, then it may be possible to make a competitive measurement of Δs, the strange quark contribution to the proton spin.

Finally, by using the same neutrino beam that was used by the MiniBooNE experiment, we will be able to directly compare neutrino cross sections off carbon ($A = 12$) and argon ($A = 40$) targets and search for a nuclear dependence of the cross section.

III. OVERVIEW OF THE LAR1-ND DETECTOR

The design of the LAr1-ND detector [5] builds on many years of LAr TPC detector R&D and experience from design and construction of the ICARUS-T600, ArgoNeuT, MicroBooNE, and LBNF detectors. The basic concept of the LAr1-ND detector, based on LBNF-type technology, is to construct a membrane-style cryostat at 110 m from the Booster neutrino source in a new enclosure adjacent to and directly downstream of the existing SciBooNE hall. The membrane cryostat will house multiple cathode plane assembly (CPA) and anode plane assemblies (APAs) to read out ionization electron signals. The APAs located near the beam-left and beam-right

Process		**No. Events**	**Events/ ton**	**Stat. Uncert.**
	ν_μ Events (By Final State Topology)			
CC Inclusive		5,212,690	46,542	0.04%
CC 0 π	$\nu_\mu N \to \mu + Np$	3,551,830	31,713	0.05%
	$\cdot\ \nu_\mu N \to \mu + 0p$	793,153	7,082	0.11%
	$\cdot\ \nu_\mu N \to \mu + 1p$	2,027,830	18,106	0.07%
	$\cdot\ \nu_\mu N \to \mu + 2p$	359,496	3,210	0.17%
	$\cdot\ \nu_\mu N \to \mu + \geq 3p$	371,347	3,316	0.16%
CC 1 $\pi^\pm$	$\nu_\mu N \to \mu +$ nucleons $+ 1\pi^\pm$	1,161,610	10,372	0.09%
CC $\geq 2\pi^\pm$	$\nu_\mu N \to \mu +$ nucleons $+ \geq 2\pi^\pm$	97,929	874	0.32%
CC $\geq 1\pi^0$	$\nu_\mu N \to \mu +$ nucleons $+ \geq 1\pi^0$	497,963	4,446	0.14%
NC Inclusive		1,988,110	17,751	0.07%
NC 0 π	$\nu_\mu N \to$ nucleons	1,371,070	12,242	0.09%
NC 1 $\pi^\pm$	$\nu_\mu N \to$ nucleons $+ 1\pi^\pm$	260,924	2,330	0.20%
NC $\geq 2\pi^\pm$	$\nu_\mu N \to$ nucleons $+ \geq 2\pi^\pm$	31,940	285	0.56%
NC $\geq 1\pi^0$	$\nu_\mu N \to$ nucleons $+ \geq 1\pi^0$	358,443	3,200	0.17%
	ν_e Events			
CC Inclusive		36798	329	0.52%
NC Inclusive		14351	128	0.83%
Total ν_μ and ν_e Events		7,251,948	64,750	
	ν_μ Events (By Physical Process)			
CC QE	$\nu_\mu n \to \mu^- p$	3,122,600	27,880	
CC RES	$\nu_\mu N \to \mu^- \pi N$	1,450,410	12,950	
CC DIS	$\nu_\mu N \to \mu^- X$	542,516	4,844	
CC Coherent	$\nu_\mu Ar \to \mu Ar + \pi$	18,881	169	

TABLE I: *Estimated event rates using GENIE (v2.8) in the LAr1-ND active volume (112 t) for a* 6.6×10^{20} *exposure. In enumerating proton multiplicity, we assume an energy threshold on proton kinetic energy of 21 MeV. The* 0π *topologies include any number of neutrons in the event.*

walls of the cryostat will each hold 3 planes of wires with 3 mm wire spacing. The wire readout arrangement is identical to MicroBooNE, with banks of cold electronics boards at the top and one vertical side of each APA. The total number of readout channels is 5,632 per side (11,264 in the entire detector). The CPAs have the same dimensions as the APAs and are centered between them. Each pair of facing CPA and APA hence forms an electron-drift region. The open sides between each APA and the CPA are surrounded by 4 Field Cage Assembly (FCA) modules, constructed from FR4 printed circuit panels with parallel copper strips, to create a uniform drift field. The drift distance between each APA and the CPA is 2 m, such that the cathode plane will need to be biased at -100 kV to create an electric field of 500 V/cm. Accurate mapping of the electric field in the drift region will be performed through a UV laser-based calibration system. The active volume is 4.0 m (width) $\times$ 4.0 m (height) $\times$ 5.0 m (length), containing 112

tons of liquid argon. The LAr1-ND design will additionally include a light collection system for the detection of scintillation light and the detector will be complemented by an external cosmic ray tagging system. In addition, we are looking into the possibility of placing shielding over the near detector should it be deemed necessary to reduce cosmogenic backgrounds.

Overall, the design philosophy of the LAr1-ND detector is to serve as a prototype for LBNF that functions as a physics experiment. While the present conceptual design described here is an excellent test of LBNF detector systems sited in a neutrino beam, the LAr1-ND collaboration is exploring innovations in this design and the opportunity to further test them in a running experiment.

A. Detector Dimensions

The LAr1-ND detector size has been optimized with respect to the preliminary design described in the LAr1-ND proposal [5]. In the original proposal the detector was designed to be located in the existing experimental enclosure that previously housed the SciBooNE experiment, at 100 m from the BNB target. The dimensions of the detector were dictated by the size of the enclosure, leading to an active volume of 4.0 m (width) $\times$ 4.0 m (height) $\times$ 3.6 m (length), containing 82 tons of liquid argon. Studies reported in Ref. [6] indicated the advantage of locating the near detector in a new enclosure, directly downstream of the existing SciBooNE enclosure at 110 m. A new building opens the question of the detector dimensions and optimizing it for physics. Enlarging the dimensions in the transverse directions has not been considered in order to maintain the 2 m maximum drift length and the height of the detector (to avoid larger excavation costs). However, Monte Carlo studies of muon containment and photon background rejection as a function of the detector length in the beam direction have been performed.

Figure 2 shows the breakdown of the fate of muons produced in ν_μ CC interactions in a fixed fiducial volume as a function of the overall active detector length. In a 4.0 m (width) $\times$ 4.0 m (height) $\times$ 3.6 m (length) detector, 53% of muons are contained (so muon momentum can be measured through calorimetric reconstruction with very good accuracy), 35% exit with a track longer than 1 m (so muon momentum is measured by multiple scattering, with less accuracy), and the remaining 12% exit with a track shorter than 1 m (so muon momentum cannot be measured). Increasing the length of the detector in the direction of the beam to 5 m increases the fraction of fully contained muons to 62%, a 17% fractional increase. The 11% minimum on the fraction of exiting muons shown in the plot is due to tracks that leave the volume through the sides of the detector, and can be reduced by tightening the fiducial volume definition.

IV. TPC DESIGN

The conceptual design for LAr1-ND is shown in Figure 3a which shows the TPC housed inside a membrane-style cryostat. The LAr active volume is a rectangular parallelepiped with dimensions of 4 m vertically, 4 m horizontally, and 5 m along the beam direction. The TPC consists of four anode plane assemblies (APAs) and two central cathode plane assemblies (CPAs), as indicated in Figure 3b. The APAs and CPAs are large-scale elements with an area of 4 m $\times$ 2.5 m each. The overall dimensions of the individual APAs are restricted to be increments of the top (192 mm) and side (222 mm) readout board dimensions. The TPC is oriented such that the Booster neutrino beam passes perpendicular to the drift direction. The TPC key

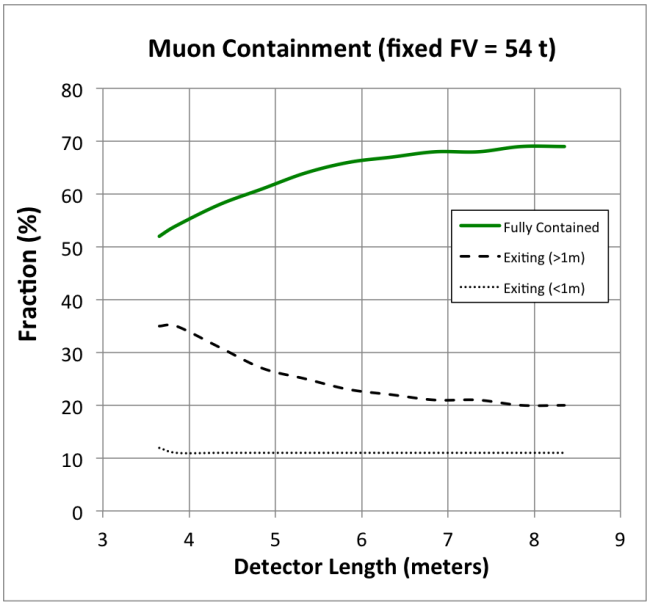

FIG. 2: *Muon containment as a function of the detector length in the beam direction.*

design parameters are summarized in Table II.

The main requirements of the TPC are:

1. The TPC volume is large enough to achieve the physics goals of the experiment. The 4 m × 4 m dimensions of the TPC active volume in the transverse (perpendicular to beam) directions and 5 m dimension in the longitudinal (along beam) direction are determined based on studies of signal containment and background rejection (see Section III A).

2. The 3 mm wire pitch is chosen, as in the MicroBooNE and ICARUS-T600 detectors, to enable electron/photon separation to be achieved with identical efficiency.

3. The APAs are constructed in a manner that guarantees no wires will break during the operational life of the experiment.

TABLE II: *LAr1-ND TPC key design parameters.*

TPC Parameter	**Value**
TPC active volume	5 m (L) × 4 m (H) × 4 m (W), 112 metric ton active LAr mass
Number of TPC cells	2 drift volumes, 2 m drift length in each
Maximum drift time	1.28 ms
Anode Plane Assembly	2.5 m × 4 m active area, with cold electronics mounted on 2 sides
Wire properties	150 μm, CuBe
Wire planes	3 planes on each APA, U & V at ±60° to vertical (Y)
Cathode bias	-100 kV at 500 V/cm drift field
Number of Wires	2816 channels/APA, 11264 wires total in TPC
Wire tension	0.5 kg at room temperature

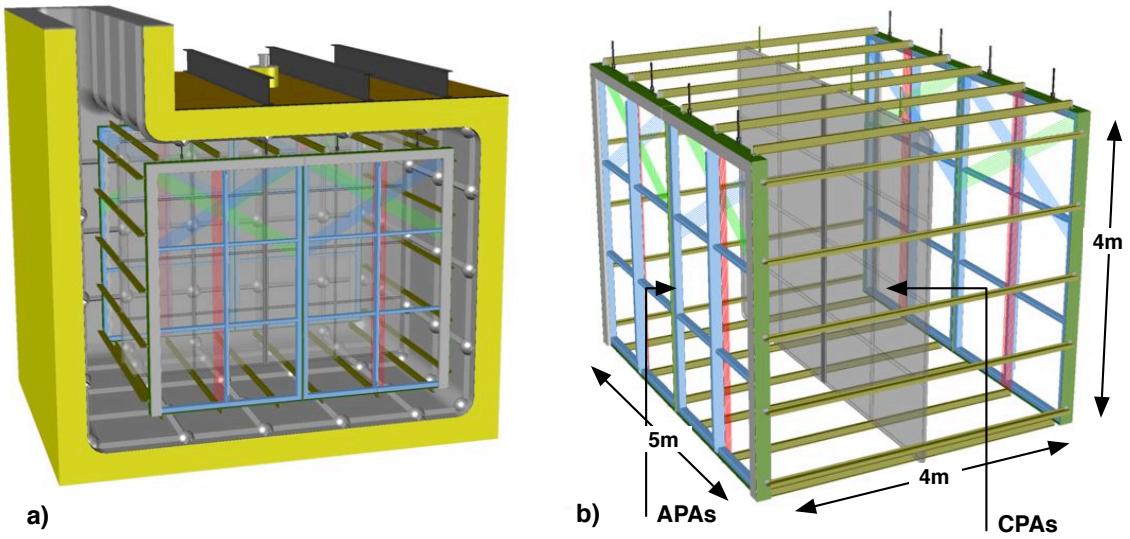

FIG. 3: *a) A conceptual design of the LAr1-ND and b) a model of the TPC, showing the four bridged APAs and the central CPAs.*

4. The high voltage system and field cage provides a uniform and stable drift field in order to capably image the entire fiducial volume.

5. The electric field everywhere inside the cryostat must not exceed 40 kV/cm to prevent breakdown [7].

A. The Anode Plane Assembly

Each LAr1-ND APA will consist of 3 planes (referred to by the direction they are oriented: Y, U and V) of 150 μm diameter Copper-Beryllium (CuBe) wires. The wire pitch and plane spacing is 3 mm, with the collection planes vertical (Y), and the two induction planes (U,V) each have wires at angles of $\pm 60^{\circ}$ from the vertical. Bias voltages of approximately -200 V, 0 V, and +500 V will be applied to the (U,V,Y) wire planes, respectively, to provide the 100% transparency condition necessary to allow all electrons to pass through the U and V planes and be collected by the Y plane.

All wires in the APAs are bonded mechanically with epoxy and terminated electrically with solder onto bonding boards made out of G10, which also provide connection to the readout electronics. The APA uses the same wire bonding method developed for the LBNF APAs, but without the continuous helical wrapping. Each wire will be tensioned at 0.5 kg per wire when the APA is at room temperature. The wires would acquire an additional 0.7 kg if suddenly cooled to liquid argon temperatures while the support frame structure is still warm, therefore a controlled cooldown rate is needed. Since CuBe has a nearly identical CTE as that of the stainless steel, the nominal wire tension will be restored once the entire APA is cooled down. This CuBe wire has a break load of approximately 3 kg at the LAr temperature, so the wire tension will be comfortably below this threshold.

In order to minimize the cost of the readout electronics, each APA has cold readout electronics on two edges only. The U wires of the two APA's observing the same drift volume are electrically connected at the joining edges via flexible jumper cables (see Figure 4). Similarly

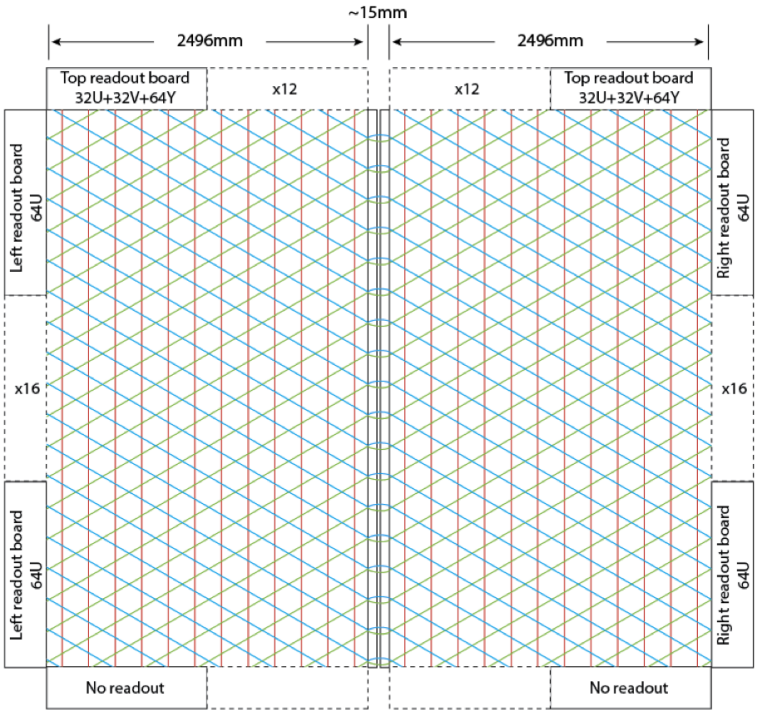

FIG. 4: *A schematic of the bridged APAs.*

for the V wires. The installation/access of the jumpers should be done before the installation of the cold electronics to avoid ESD damage to the ASICs. The jumper cables use industry standard gold plated pin and socket connections, similar to all electrical interconnects between the cold electronics boards. Although the jumpers may increase the risk of open circuit on the wire readout somewhat, its benefits in the reduction of readout channel count, and the APA size outweight the risks. Nevertheless, one of our early design efforts will be the selection and evaluation of the interconnect components at the cryogenic temperatures. A special set of readout electronics may be needed to read out the joining edge of an APA during individual APA testing.

In this design there is a gap of 15 mm between the two active apertures of the APAs which creates a "dead" readout region. To overcome this issue there is an option to insert a printed circuit board in the gap between the two APAs, and bias the circuit board strips with a voltage distribution such that the incoming electrons will be deflected away from this gap and land in the active region of the wire frame. In this field configuration, there will be no electron loss, but reconstructed inclined tracks will appear distorted at this gap. As this region has a fixed distortion, it can be easily mapped out and corrected (see Figure 5). This field shaping concept will be implemented at one section of the LBNE 35ton TPC and evaluated during the LBNE 35ton Phase II operation.

Figure 6 is a view of an upper outer corner of an APA. Three layers of wire bonding boards are stacked on the front face of the frame. The wires are bonded to each board at the leading edge with epoxy, and then soldered to copper pads on the boards. Copper traces on the wire bonding boards bring the wire signal to the cold electronics boards mounted on the two outside edges of the frame. Only the wires on the joining edge of the APA are bonded on "LBNE" style grooved boards (Figure 5a, 7). This configuration minimizes the number of grooved boards which are labor intensive to fabricate, while maintaining a relatively small dead space between

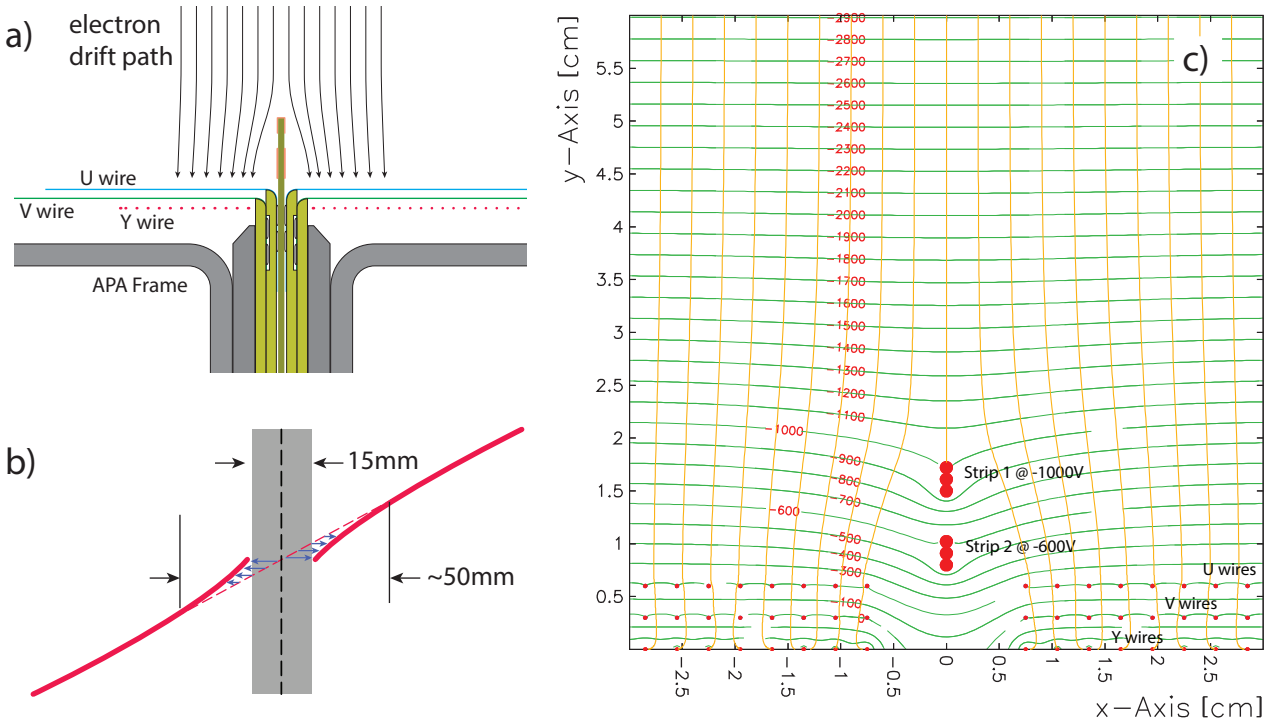

FIG. 5: *a) A concept to eliminate the dead region between the two APAs by adding a few properly biased electrodes at the center of the gap to divert the electrons to the nearby active regions. b) The distortion on the reconstructed tracks. c) A Garfield simulation of the electron drift lines in a two strip configuration.*

APAs.

High voltage capacitors and high value resistors are needed for each readout channel with a bias voltage (U & Y). These components can be integrated on the wire bonding boards (MicroBooNE style), or mounted on intermediate CR boards between the wire bonding boards and the FEE boards (LBNE style).

The four stainless steel APA frames are required to be flat and to have rigid tolerances. The distributed load on the frame is calculated to be 250 kg/m. Since this load is applied to one side of the frame only, it has the tendency to bow the frame. This in turn could make the wire plane spacing non-uniform over the entire opening, resulting in different electron transparency. The transparency can be restored by over biasing the wires, but we should keep the flatness of the frame to better than $\sim$ 0.5 mm to avoid very high bias voltages. Since the APA frames are outside of the TPC's active volume, it is straightforward to design the frames to be stiff against such distortions. Adjustment of the wire bonding boards can also be made at APA assembly time to further improve the wire plane precision over fabrication tolerances in the APA frames.

A prototype LBNE type frame with dimensions 1.5 m$\times$ 0.5 m has been designed and fabricated at Sheffield University to prototype the manufacturing process, which minimizes distortions and leads to significant improvements in flatness. For the full LAr1-ND APA frame, a four-stage process is envisioned: i) secure the whole assembly to a purpose built fabrication jig during tack welding; ii) normalization of the structure (stress relief) to prevent buckling; iii) machine and drill all mounting points for additional components; and iv) chemical passivation to remove contaminants.

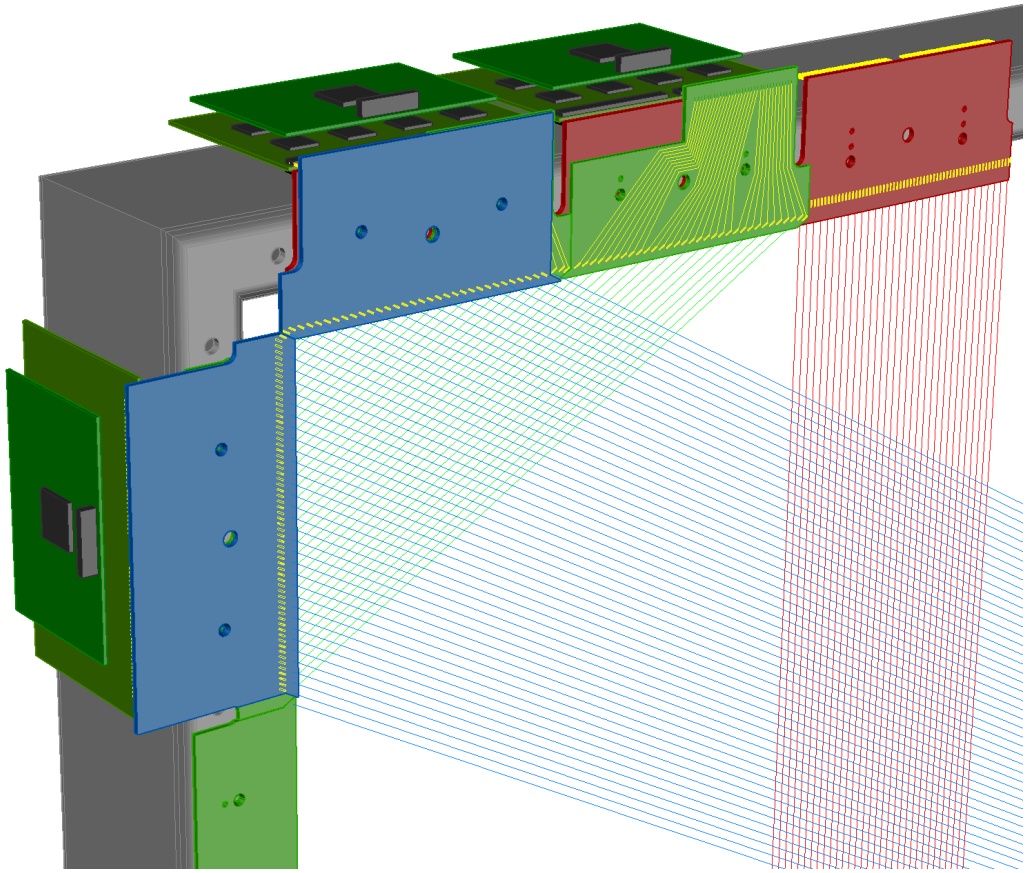

FIG. 6: *A conceptual design of an upper outer corner of an APA showing the different layers of wire bonding boards on the top end side of the APA frame. The cold electronics boards are connected to these wire bonding boards. Metal covers may be installed over the electronics boards to reduce noise pickup and contain the boiled argon bubble streams.*

B. The Cathode Plane Assembly

The CPA has the same dimensions as the APA and consists of a stainless-steel framework. The surface of the CPA panels will be either a solid stainless steel sheet or a highly transparent wire-mesh-plane. The requirements of the light collection system will dictate which CPA surface is used. For example, a double layer mesh cathode module enables TPB coated reflector foils to be mounted in between the mesh planes. This configuration allows the polymer foils to contract freely during cool-down.

During manufacture, all the CPA surfaces will be carefully polished in order to avoid any sharp edges that could lead to electrical discharge. If a transparent type CPA is chosen the mesh will be tensioned and mounted between two steel frames in order to enclose the sharp edges of the mesh (see Figure 8). G10 mounting connectors will be pre-installed on the outer edges of the CPA to allow integration of the CPA and the Field Cage Assembly (FCA) modules. Finally, a HV cup will be integrated to allow connection of the HV feedthrough to the CPA.

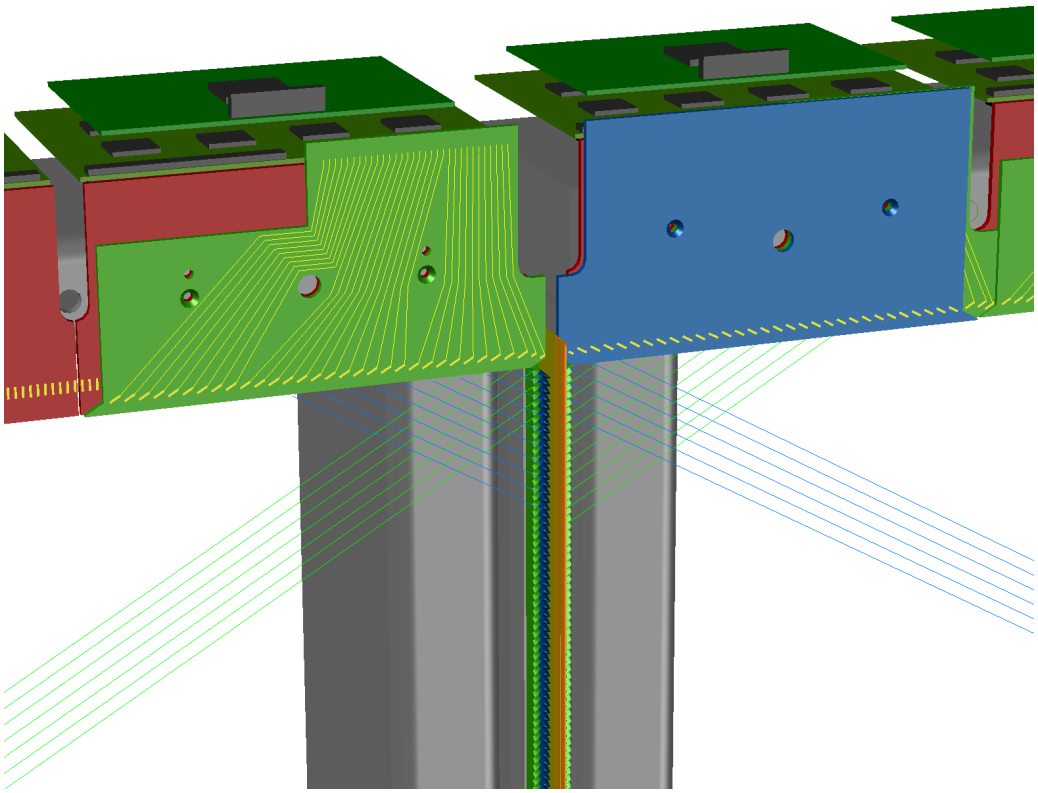

FIG. 7: *A closeup view of the gap between the two APAs showing a possible implementation of the electron diverter concept*

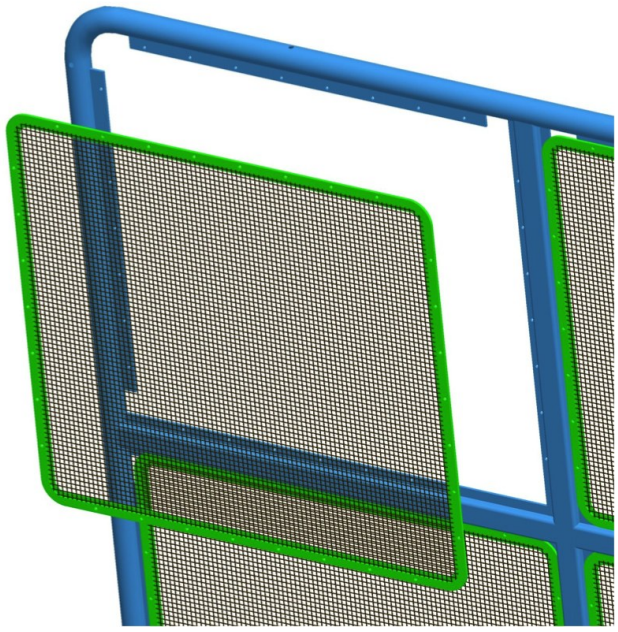

FIG. 8: *A model of the CPA corner, showing the mesh into the frame assembly.*

C. The High Voltage Feedthrough

A single high voltage feedthrough is installed through a cryostat penetration to connect the high voltage power supply to the CPA. To provide the 500 V/cm drift field over the 2 m drift distance the CPA will sit at a potential of -100 kV. To ensure safe and reliable operation, the HV feedthrough is constructed with a HV rating of no lower than 120 kV in liquid argon. The design of this feedthrough is based on the design of the ICARUS/ MicroBooNE feedthrough. To avoid outgassing of impurities, the feedthrough uses a central stainless steel conducting core within an Ultra-High Molecular Weight Polyethylene (UHMW-PE) insulator surrounded by a stainless steel grounding sheath. UHMW-PE has a high dielectric strength, ensuring a compact feedthrough design, and its high-thermal expansion coefficient relative to stainless steel allows the vacuum seal to be cryo-fitted. The outer stainless steel sheath will terminate prior to the contact to the CPA to prevent electrical breakdown. As in the ICARUS/MicroBooNE design, the feedthrough will be removable from outside of the cryostat in the event that it needs to be replaced. A 150 kV power supply (Glassman LX150R12) in conjunction with a noise filter will be utilized as in MicroBooNE.

D. The Field Cage

The HV drift cage must provide a uniform 500 V/cm electric field over the TPC active volume to maintain linearity between drift distance and time of ionization. The field cage gradually steps the voltage from the -100 kV applied to the CPA up to ground voltage. It will be made from 1.6 mm double sided Cu clad FR4 PCBs, similar to the 35t LBNE prototype. The double sided Cu cladding effectively ensures that the inter-strip capacitance is increased thus minimizing over voltage conditions between the CPA and field cage strips in the event that the CPA or the field cage discharge to ground. A photo of the 35t field cage panels is shown in Figure 9. Slits between the Cu etched strips ensure good liquid argon flow. Additionally, in order to accommodate the laser beam calibration system (see Section VI) the side field cage walls will have two openings 50 mm ID in each drift volume at the half-height. A resistor divider chain will supply the potential for the field cage electrodes. To reduce the field distortion caused by a possible resistor failure, four equal value 1 GΩ resistors, with each resistor rated at 5 kV and 1 W, will make parallel connections between neighboring electrodes. These resistors will be located on the inner wall of the TPC since the electric field in this volume is lower than that outside the TPC.

Surge protection elements will be placed in parallel with the resistor divider chain to provide redundant protection to the resistors should a catastrophic voltage condition begin to arise in the chain. This technique was instigated by the MicroBooNE collaboration and shown to provide a reliable method of handling high-voltage breakdown issues [8].

E. Installation Procedure

There are two installation options for the TPC. One option is to pass all TPC components through the cryostat chimney; this would require completion of the cryostat prior to the TPC installation and the dimensions of all internal components would be restricted by the size of the chimney. The second and more favorable option is to hang all the TPC assembly from a main lid before sealing. This option allows for parallel construction of the TPC and cryostat.

FIG. 9: *A photo of the 35 ton LBNE prototype field cage.*

However, this creates the necessity for the building housing the detector to be tall enough and an adequate load capacity crane would be needed.

F. Quality Control and Quality Assurance

A QA program will be performed at Lancaster University to confirm the APAs constructed in the UK behave as expected when cooled to 77K using liquid nitrogen. These results will verify the design and manufacturing process of all APAs. Cold tests will be carried out in a purpose-built ~ 3 m $\times$ 4 m $\times$ 0.2 m thermal cryo-vessel, large enough to contain the full-scale APA. The vessel will be constructed from stainless steel with polystyrene insulation. The vessel, with the APA inserted, will be cooled with gaseous nitrogen prior to filling with liquid nitrogen. The thermo-mechanical measurements will include: a survey of the bending and distortion of the APA frame structure and comparison with FEA calculations; vibration frequency based APA wire tension measurements; and resistance measurements to test electrical integrity.

Travelers will be provided for all TPC components shipments detailing contents and relevant instructions.

G. Risks

Breakage of a single wire can jeopardize the detector's functionality, so a QA procedure will be followed to ensure the tension of the wires is never higher than that of their desired warm tension of 0.5 Kg, and wires are not subject to any kinking that could reduce their strength. The tension of each wire installed on the APAs will be measured using a laser feedback system developed as part of the LBNE 35-ton project, and subsequently used by both MicroBooNE and LArIAT during TPC construction.

Breakdowns in the liquid argon volume can produce over-voltage conditions across resistors in the field cage, which if damaged could produce distortions in the drift-field. Surge protection

devices, as developed by the MicroBooNE experiment, will be present mitigating the risk to the resistors.

V. TPC ELECTRONICS, DAQ AND TRIGGER

A. Introduction

The aim of the TPC readout is to digitize, compress losslessly and record the TPC signals upon the reception of a variety of triggers such as neutrino beam and cosmic rays triggers generated by the light detection system as well as external scintillation counters, calibration and random strobe triggers. In order to fully reconstruct cosmic rays entering the drift space during an event drift time, data arriving from -1.28 msec before the trigger to +2.56 msec after the trigger (a total of 3 maximum drift times) will be recorded and compressed losslessly at each event. In a parallel stream, and as useful R&D for LBNF, the readout will continuously record data, compress it and store it for a few hours awaiting for a possible supernova alert from the SNEWS network.

The block diagram of a single TPC readout channel is outlined in Figure 10. The signal from each wire is pre-amplified and shaped by a CMOS analog front end ASIC, then digitized by a CMOS ADC ASIC inside the cryostat. The digitized signal is sent to an FPGA, which aggregates data from multiple ADC chips and multiplexes it to high speed serial links. The serial data is sent over cold cable through a feed-through to the warm interface board installed outside the cryostat on top of the signal feed-through. The warm interface board receives the electrical serial data from the cold electronics and converts it to optical signals for transmission over a fiber optical link to the TPC readout module, housed in a crate. Once the signal arrives at the TPC readout module, it is processed in an FPGA for compression, reduction, and storage. Processed data is buffered on board temporarily and then transmitted to DAQ PCs through the crate backplane and optical links. Data received on PCs is stored in hard drives for further analyses.

The design of the front end electronics, the TPC readout and the trigger is described in the next sections. A summary of the numbers of modules needed and of the spares as well as their distribution is reported in Table III.

B. The Front End Electronics

The LAr1-ND front end electronics is comprised of three parts: cold electronics, warm interface electronics and signal feed-through. The cold electronics will be installed on the TPC anode assembly and operated in LAr. The digitized detector signal will be sent to the warm interface electronics over cold cable. The warm interface electronics will be installed on the top signal feed-through assembly, and interface to both cold electronics and back end readout electronics and the DAQ system.

1. Cold Electronics

The LAr1-ND TPC will have two APA modules, on each side with 5,632 channels, a total 11,264 readout channels for the whole TPC. The large number of readout channels required to instrument the LAr1-ND TPC motivates the use of CMOS ASICs for the electronics. Both

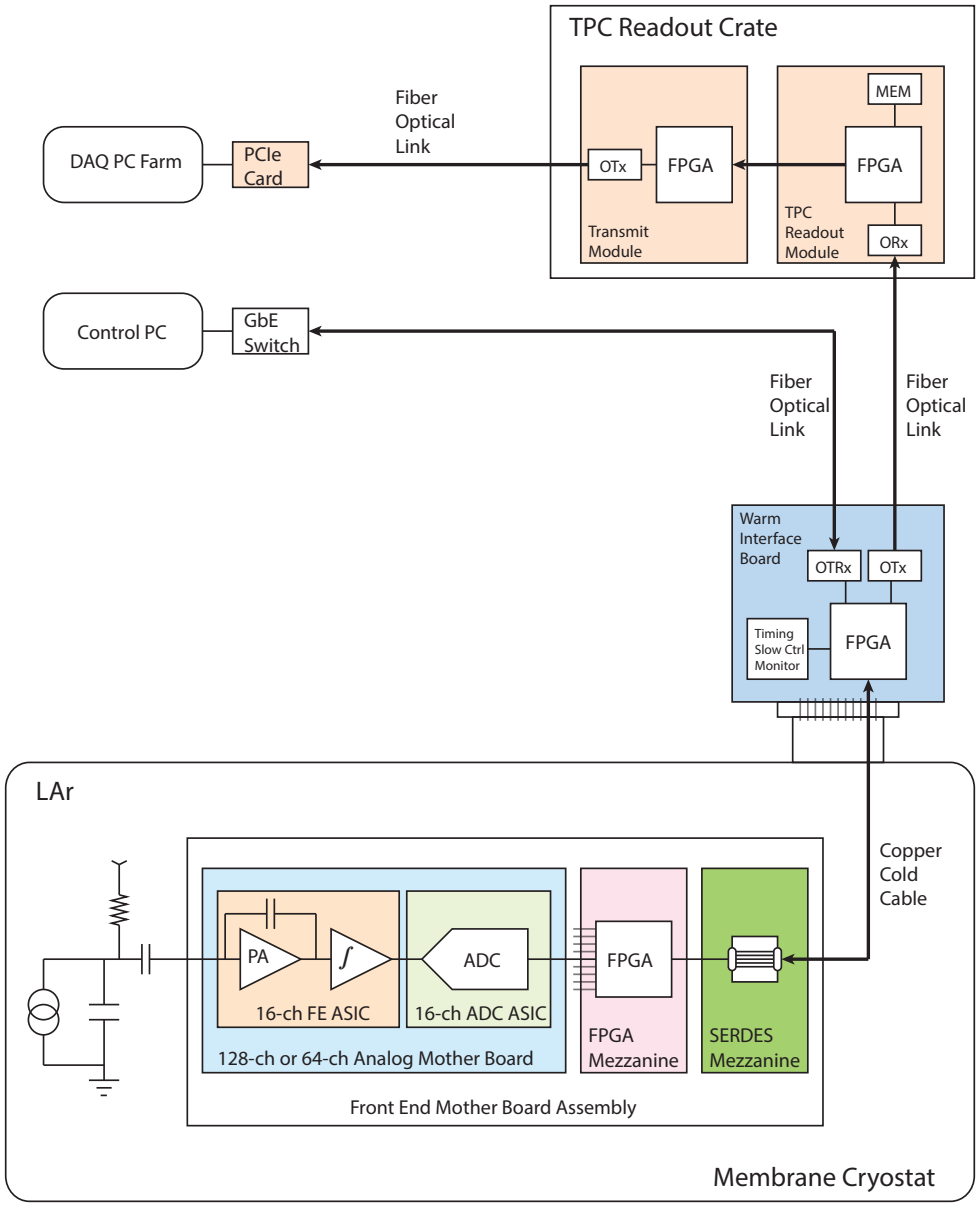

FIG. 10: *Information flow of a single TPC readout channel.*

analog FE ASIC and ADC ASIC, to a large extent, have already been developed for LBNE, and analog FE ASIC is being used in MicroBooNE. The entire front end electronics chain is immersed in the LAr and operates at 87 K to achieve an optimum signal to noise ratio. It is composed of a 16-channel analog FE ASIC providing amplification and shaping, a 16-channel ADC ASIC implemented as a mixed-signal ASIC providing digitization, buffering and the first stage of multiplexing, a FPGA providing the second multiplexing stage, and voltage regulators. Analog FE ASICs, ADC ASICs plus a FPGA implementing multiplexer, clock, control and monitoring circuitry comprise a single 128-channel or 64-channel front end mother board

Module	Channels per Module	Distribution	Number of Modules needed	Number of Spare Modules	Number of Modules
Front End Modules (FEM)	64 wires/FEM	16 FEM/crate	176	18	194
Crates			11	2	13
Backplane		1 Backplane/crate	11	2	13
XMIT		1 XMIT/crate	11	2	13
Crate Controller (CC)		1 CC/crate	11	2	13
PCIe		3 PCIe/crate	33	4	37
Trigger module			1	2	3
Analog FE ASIC	16 wires		704	96	800
ADC ASIC	16 wires		704	96	800
128-ch Mother Board	128 wires		52	6	58
64-ch Mother Board	64 wires		72	8	80
FPGA Mezzanine	128 or 64 wires		124	14	138
SERDES Mezzanine	128 or 64 wires		124	14	138
Warm Interface Board	704 wires		16	4	20
Service Board	2,816 wires		4	2	6
Signal Feed-through	2,816 wires		4	2	6
Cold Cable	2,816 wires		4	2	6

TABLE III: *Numbers of modules needed and of spares as well as their distribution.*

assembly. The FPGA on each motherboard will transmit data out of the cryostat on twinax copper pairs running at multiple Gbit/s through a feedthrough to the warm interface electronics, and receive programming instructions and timing information from the warm interface electronics as well.

Each side of the TPC has two APA modules, which are interconnected along the adjacent side. Each APA module will have 31 front end mother boards on two sides. 13 boards will be located on top of the TPC with each board processing 128 channels. 18 boards will be on the side without interconnection, with each board housing 64 channels. A block diagram of the 128-channel front end mother board is shown in Figure 11. Both analog FE ASIC and ADC ASIC have been designed and fabricated in a commercial CMOS process (0.18 μm and 1.8 V). This guarantees a high stability of the operating point over a wide range of temperatures, from room temperature to 77 K. The ASICs are packaged in a commercial, fully encapsulated plastic QFP 80 package. A minor revision of the analog front-end ASIC, to further improve the robustness and simplify the system design, including internal pulse generator, smart reset and improved input protection is being planned. It will greatly simplify the design of the electronic calibration system.

The Cold FPGA will interface to analog FE ASICs and ADC ASICs on the analog mother board. It will control and monitor ASICs, and receive data from ADCs. Once data arrives at the FPGA, a second stage multiplexer will be implemented to further reduce the number of data links to outside of the cryostat. The design is to support transparent data readout without any compression over 2Gbit/s serial links. An efficient zero-suppression scheme can be implemented in the FPGA to greatly reduce the total data volume if proven to be feasible and necessary. Each mother board processes 128 or 64 detection channels. The clock will come in through RX links while data is sent out over TX links. Voltage regulators used on board

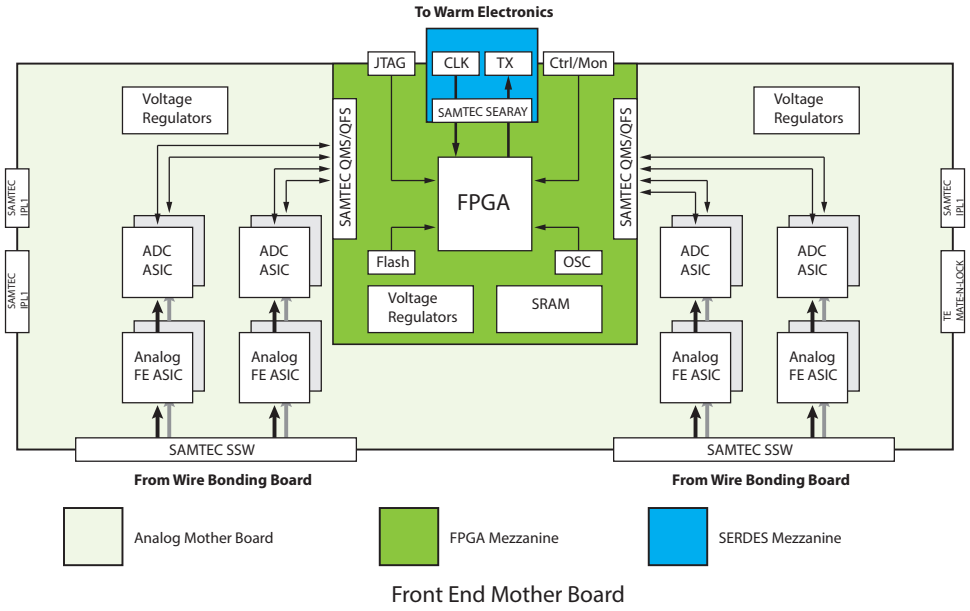

FIG. 11: *Block Diagram of Front End Mother Board Assembly.*

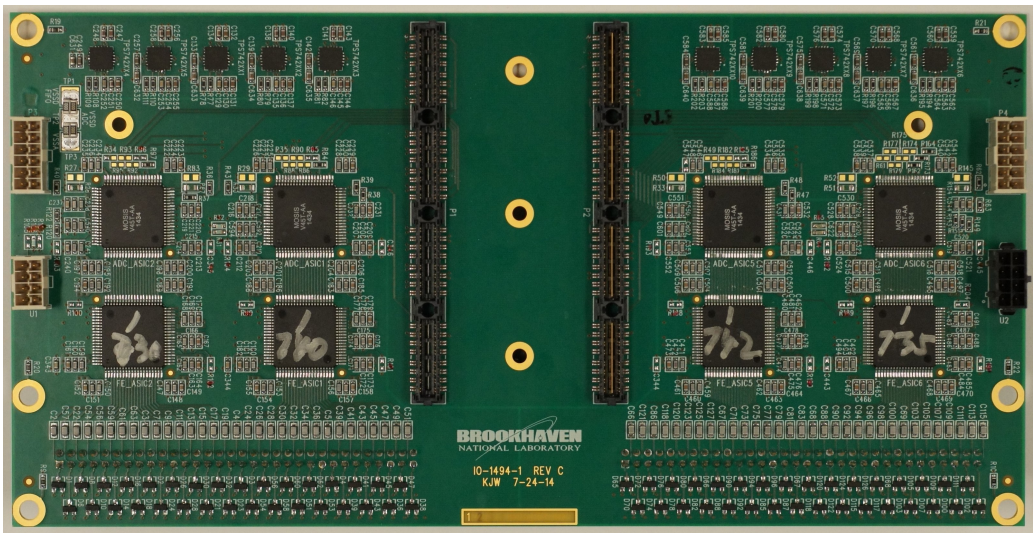

FIG. 12: *Prototype 128-ch analog mother board designed for LBNE 35ton prototype TPC.*

have been qualified in liquid Nitrogen. On the board, SRAM is used to temporarily buffer events if a more sophisticated algorithm is used to process data. A commercial SRAM chip working in cryogenic temperature has also been identified. The estimated power dissipation is 20 mW/channel. The ALTERA Cyclone IV GX FPGA will be used in the FPGA mezzanine design. It has been tested in LN2 successfully, both fabric logic and a high speed transmitter are working properly at cryogenic temperature.

The prototype front end mother board is being designed for the LBNE 35 ton prototype. The picture of the prototype 128-ch analog mother board is shown in Figure 12 and prototype FPGA mezzanine is shown in Figure 13. SERDES mezzanine is a passive adapter board, which will be plugged on the FPGA mezzanine to interface to cold cable. The candidate cold cable

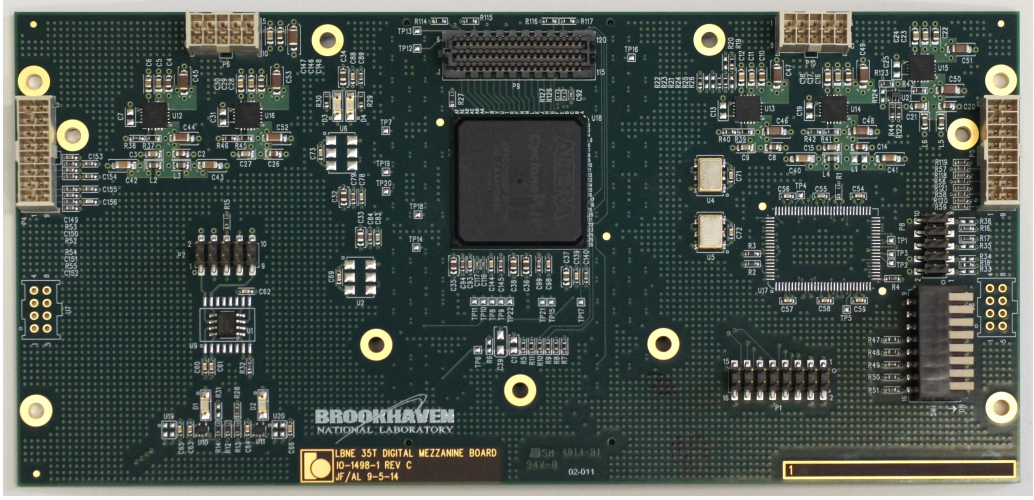

FIG. 13: *Prototype FPGA mezzanine designed for LBNE 35ton prototype TPC.*

is made by Gore using twinax cable and ERNI hard metric connector. The 50ft Gore twinax cable has been tested with feed-through pin carrier running at 2 Gbit/s successfully.

2. Warm Interface Electronics

The detector signal is digitized inside the cryostat. After multiplexing in FPGA, it is sent out of the cryostat over copper serial link to the warm interface electronics installed on the top of the signal feed-through. The warm interface board will be the bridge between the cold electronics and back end readout electronics and DAQ system.

The warm interface board will use ALTERA Cyclone V FPGA, which will receive high speed serial link coming out of cryostat, perform data preparation, then send the data to the readout and DAQ system through fiber optical links. On board FPGA has computing power to do further data processing if necessary before sending the data to downstream electronics. By default, data interface board will send data over a 2 Gbit/s link to the TPC readout module, which processes un-compressed 64-ch worth of data. The whole TPC will require 176 fiber optical links to carry data from 11,264 TPC channels. A 12-ch parallel fiber optical link will be used to minimize the volume required on board, requiring a total of 16 fiber bundles. This will ease the design of the electronics assembly on the top of the signal feed-through.

Timing, control and monitoring are also functions of the warm interface electronics. The system clock and synchronization signal will be distributed from warm interface board to the front end mother board assembly. Slow control and monitoring information will also be communicated between the warm interface board and the front end mother board assembly, using an I2C like protocol. The front end mother board assembly can be remotely programmed and monitored through a control PC. The communication between the warm interface board and control PC is by Gigabit Ethernet over a fiber optical link.

The front end analog ASIC has a built in calibration capacitor, to facilitate the electronic calibration. With plans to revise the front end analog ASIC adding a built-in calibration pulse generator, there is no need to distribute the calibration pulse signal from outside the cryostat. This will greatly simplify the system design.

The link between warm interface electronics and back end readout electronics and control

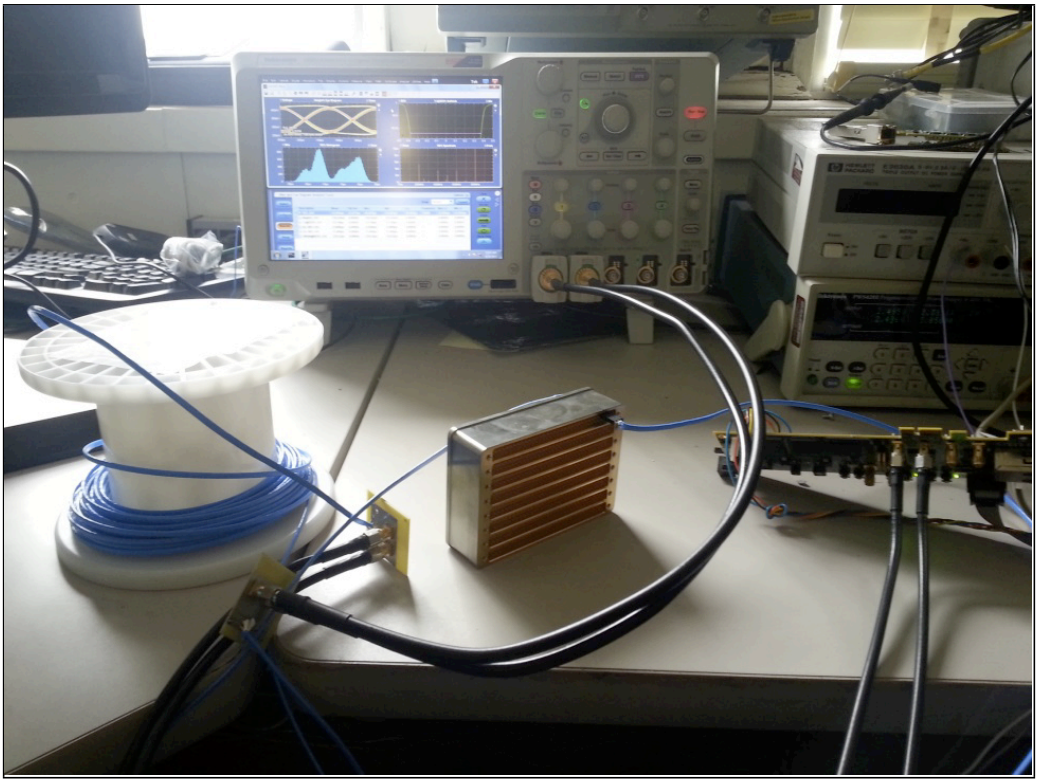

FIG. 14: *ATLAS pin carrier is tested with Gore cable for 2 Gbit/s signal transmission.*

system is only through fiber optical links. This effectively eliminates the possibility to have ground loops between the detector and the DAQ system.

Both cold electronics and warm interface electronics will be powered by a floating low voltage power supply. It is planned to have a service board installed on the top of the signal feed-through. The service board will be responsible for power management and distribution.

3. Signal Feed-through

The signal feed-through design has to consider two important factors: 100% hermeticity and high speed signal transmission capability. The ATLAS style pin carrier [9] shown in Figure 14 is designed for a LAr Calorimeter and its hermeticity has been certified. It has also been used for the MicroBooNE signal feed-through design. Since the pin carrier design is available, no additional engineering design is needed. The pin carrier is suitable for both warm flange and cold flange if LAr1-ND decides to use double flanges setup to improve the efficiency of the purification system. The manufacturer of the pin carrier has been contacted; they are still available and capable of building the same type of pin carriers with reasonable cost.

Two 8-row pin carriers and two 7-row pin carriers will be welded on a 14-inch conflat flange with a Faraday cage mounted on the top to provide the shielding for warm interface electronics. A picture of the flange with pin carriers welded on is shown in Figure 15. There will be four signal feed-throughs for LAr1-ND TPC readout. Each feed-through is used to read out one APA of 2,816 channels. A total of 44 serial links on each feed-through will come out of the cryostat running at 2 Gbit/s. Considering redundancy, ground pins and fiber organization, it will require 8 64-pin rows. The warm interface board will need proper cooling; it is envisioned

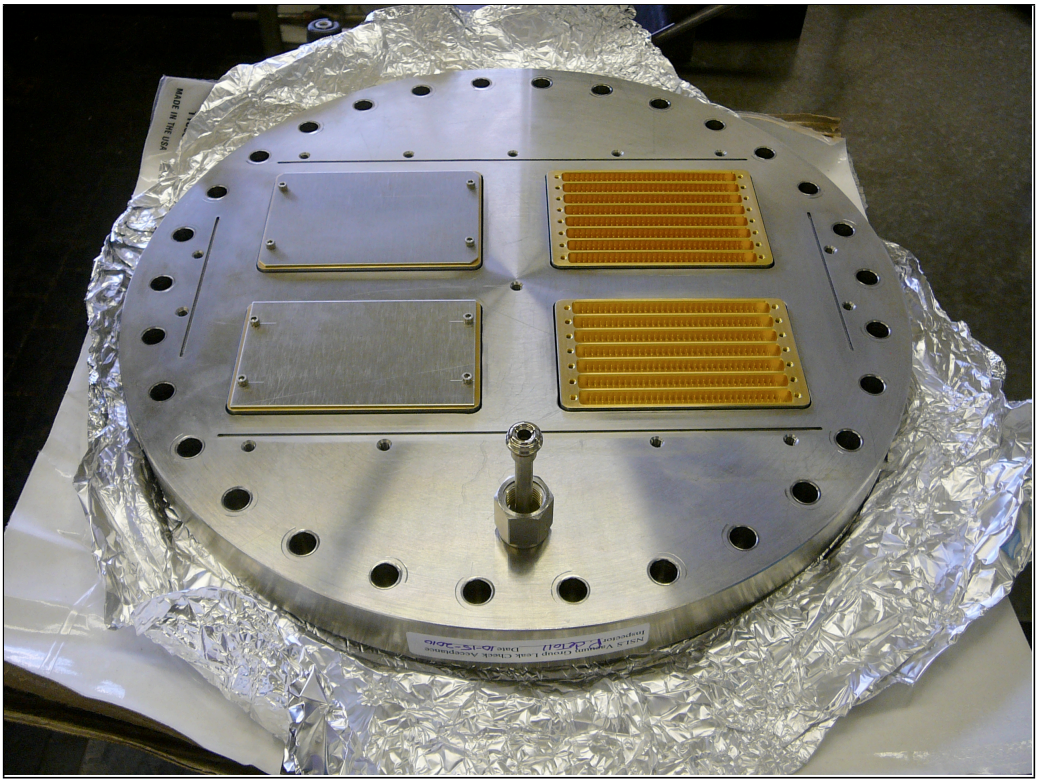

FIG. 15: *ATLAS pin carriers are welded on flange.*

that each board will occupy two pin carrier rows to allow sufficient air flow. The service board will occupy another two rows for power management and distribution. Therefore, the signal feed-through flange with 1920-pin, 30-row pin carriers is enough to handle one full anode plane assembly. It will be investigated if the readout of two APAs on one side of TPC could be fit on the one signal feed-through assembly.

C. The TPC readout

In MicroBooNE, the TPC signals are digitized outside of the cryostat in a board developed by BNL and joined to a Nevis board, the FEM, that provides the compression, storing and trigger application. In LAr1-ND the signals will be digitized within the cryostat and after emerging from the feedthrough, will go through a copper to optical transceiver and arrive on optical fibers at an adaptation of the MicroBooNE FEM Nevis boards. The FEMs will each receive signals from 64 wires and will be modified to include an optical to copper converter AFBR-59R5LZ and a deserializer TLK2501IRCP. The signals will then be treated in exactly the same way as in MicroBooNE, thus capitalizing on the extensive Nevis hardware and firmware design and development performed for MicroBooNE

A total of 176 FEMs will be required and will be housed in eleven 6U crates, sixteen 64-channel FEMs per crate. The crates each also house a fast data transmission module (XMIT) and a crate controller (CC) used for parameter transmission to the FEMs and for a slow debugging mode readout. A MicroBooNE crate layout is shown in Figure 16.

The digitized data stream is shown in Figure 17. The FPGA stores the data from 64 wires sequentially in time in a 1M x 36 bit 128 MHz SRAM memory, grouping two ADC words

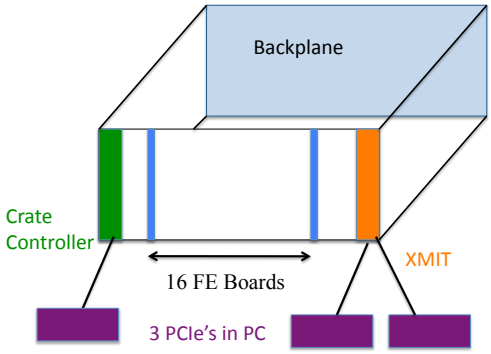

FIG. 16: *A readout crate showing, from left to right, the crate controller, up to 16 FEM modules, the XMIT and the 3 PCIe cards used for communicating with the crate and resident in a PC.*

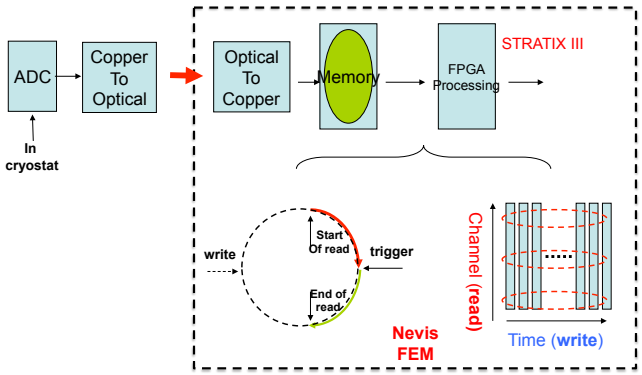

FIG. 17: *The Nevis FEM data flow, showing the circular buffer and the "write" in time order and "read" in channel order scheme.*

together in each 36 bit memory word. This requires a data storage rate of (64/2) x 2 MHz = 64 MHz. Since data reduction and compaction algorithms rely on the sequential time information of a given wire, the data readout out from this SRAM memory takes place in wire order in alternate clock cycles, again at the rate of 64 MHz. The SRAM chip size and memory access speed permit continuous readout of the TPC data. The data is arranged in frames of 1.28 ms, the maximum drift time. Since the readout clock is not synchronous with the accelerator spill time, the 3.84 ms worth of data relevant to an accelerator neutrino event spans four 1.28 ms long frames. In order to reduce the amount of data being transmitted, the FPGA trims the four frames to span the exact 3.84 ms required. Experience with a Fermilab test stand demonstrates that on any given wire, successive data samples vary relatively slowly in time. In most cases, two adjacent data samples either coincide or differ by one ADC count. Huffman coding provides for lossless data compression by taking advantage of this slow variation of the data stream. For accelerator neutrino events, lossless Huffman coding compression yields a compression factor of eight to ten and proves sufficient; but for the continuous supernova data, further compression by about an additional factor of ten, is necessary to limit the size of the data sample and to match disk writing speeds, resulting in unavoidable data loss. A method called dynamic decimation (DD) handles this case. The DD scheme relies on recognizing regions of interest (ROI) in the data stream that contain waveforms corresponding to drift charges. Parts of the data stream

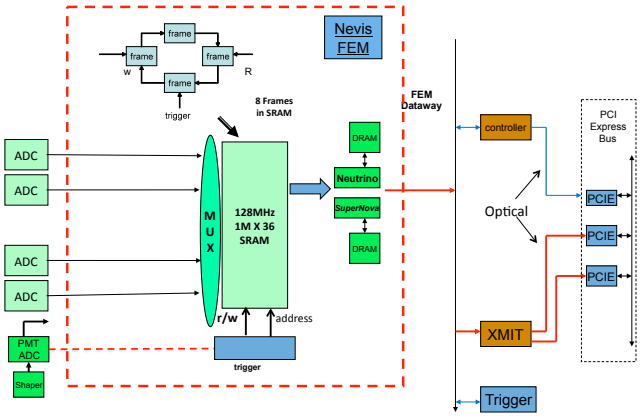

FIG. 18: *The Structure of the Nevis readout system: FEMs, dataway, XMIT, crate controller and three PCIe cards PC resident.*

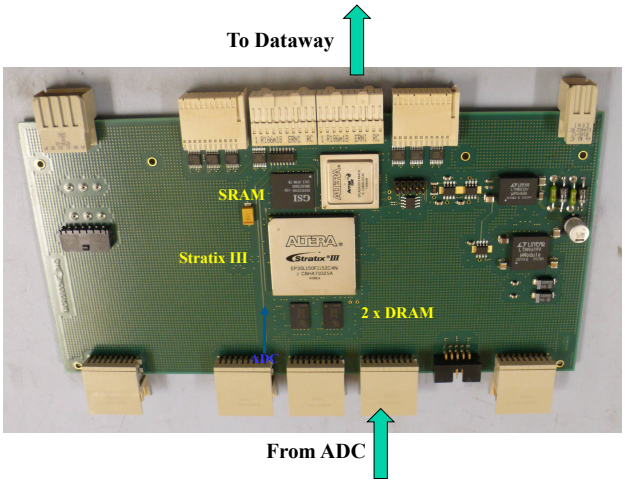

FIG. 19: *The MicroBooNE Nevis FEM.*

not containing ROI contribute to pedestal determination. In DD the FPGA samples the ROI data at the same rate as accelerator data, but reduces the pedestal sampling to a much lower rate (e.g. 1/16). The final data record of a wire contains full coverage in time, with or without drift signals from a charged track. A too-high threshold for ROI can result in loss of resolution for small signals, but the data still appear as pedestal, although sampled at a lower rate. An independent Huffman coding stage further reduces the data volume after dynamic decimation. After going through their respective compression schemes, the beam and supernova data are stored in two separate DRAM buffers as shown in Figure 18. The data is then transmitted to the crate backplane dataway on connectors shown on the right of the schematic. A photograph of the Nevis FEM board currently in use in MicroBooNE is shown in Figure 19. The transmission is controlled by the XMIT module. Each XMIT module includes two optical links, one used for the triggered data stream and the other for the continuous supernova data stream. These links connect to optical transceivers housed on two PCI Express interface cards developed at Nevis for use in ATLAS and resident in a PC. Each crate is connected to a dedicated PC (the sub-event PC). The two transceivers on the interface cards handle 6.4 GB/s traffic and connect to a 4-lane PCI Express bus, with each lane accommodating 2.5 GB/sec. The XMIT module

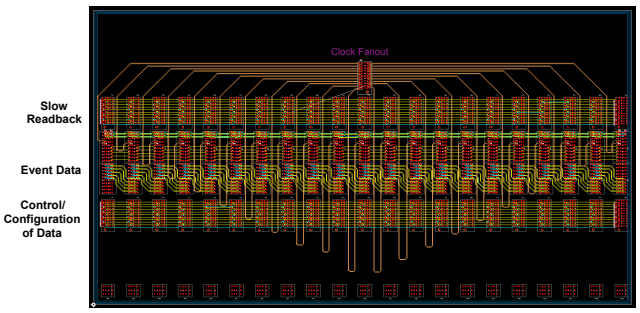

FIG. 20: *The Readout crate backplane.*

transmits data to the PC based on the token passing technique. The XMIT module generates the token and passes it to the first FEM module. This module receives the token and transmits its data, if any. The data transits from one board to the next on the crate backplane until it reaches the XMIT module. The token passes on to the next FEM module when an active FEM finishes transferring its data. Since a module only drives the data to its neighbor, it forms a point-to-point short link. Data can flow at rates up to 512 MB/sec on this path, a factor of ten faster than the expected traffic on this dataway. Figure 20 shows the layout of the crate backplane. In addition to the token passing dataway, a secondary bus serves to download the FPGA codes and initiate data/parameter readback via the crate controller and a third PCI Express card in the PC. This slower readback can be used to read out the FEM without the XMIT, a useful feature for system development, for operating a lightweight test stand, and for other purposes.

An additional PC, the event-building PC, collects the triggered data sent to it by the eleven sub-event PCs and builds triggered events through a switch. Each sub-event PC also stores the supernova data in circular buffers large enough to accommodate a few hours of continuous data. The buffers are resident in disk drives that can accommodate 100 MB/sec writing speeds, but for which we have assumed a more conservative 50 MB/sec by providing an overall supernova compression factor of 80-100.

D. The Trigger Board

The trigger board (TB) flags time frames that must be treated differently than those for continuous reading of supernova events. The light detection system generates one or more triggers based on the detector signals. Example trigger conditions include: sum of all light detector pulse heights above a threshold, sums of groups of light detector pulse heights above a lower threshold, and number of light detectors above the threshold satisfying a multiplicity requirement. Each trigger condition receives a code ranging from 1 to n, with n likely not exceeding 7, and 0 meaning no trigger. This code is transmitted serially one bit at a time to the TB on one cable as shown in Figure 21. A second cable carries a marker to identify the first bit of a trigger code transmission.

Booster and NUMI beam gates also input to the TB, where they can be placed in coincidence with light detector triggers to flag neutrino interaction candidates. Valid light detector triggers enter a logical OR with other utility triggers sent to the trigger board to form calibration triggers for the electronics, random triggers for noise measurement, off-beam triggers for cosmic ray response studies, and others as deemed necessary. All inputs to the trigger board will be

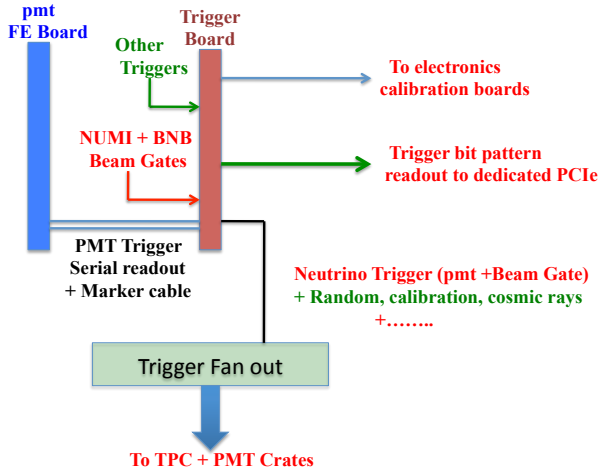

FIG. 21: *The MicroBooNE trigger scheme.*

via front panel LEMO connectors, as will the trigger output. An OR of all triggers passes to a fan-out module on a single cable, and from there is distributed to all crate controllers, and, through the crates backplane dataway, to the FEMs. Upon receiving a trigger, an FEM inhibits its supernova readout mode with its associated decimation, initiates the finer-grained readout scheme and directs the data to the appropriate readout path. Activation or masking of each of the trigger modes will be computer controlled as will the setting of the various trigger thresholds and conditions. The actual cause of the trigger will be available at the event building stage and off-line, as this information will be read out as a bit pattern from the TB via an optical fiber connected to a PCIe card resident in the sub-event PC connected to the crate housing the TB.

E. An Alternative Scheme

An alternative scheme of TPC front end electronics, readout and DAQ system is shown in Figure 22. The front end electronics could adopt the cold digital ASIC which will be developed for LBNE, if it becomes available in time. The only change is the FPGA mezzanine will be replaced by a cold digital ASIC mezzanine. It is also possible that a small section of TPC readout to be instrumented by a digital ASIC for R&D purposes if the design is not sufficiently mature will be installed on the detector. The alternative TPC readout module will use a more advanced FPGA to process 256 channels of detector signals, it will greatly simply the system design and the number of readout crates will be reduced by a factor of 2-3. Also the modern USB 3 link could be used to replace the optical fiber link with a custom designed PCIe card, for data transmission to a DAQ PC farm.

VI. UV LASER-BASED FIELD CALIBRATION SYSTEM

A. Calibration of Drift Field by UV Laser Beam

The knowledge of the electric field inside the drift volume of a TPC is a key aspect for performing subsequent event reconstruction. Since distortions of particle tracks due to field non-uniformities are indistinguishable from particle multiple scattering, they affect the accuracy

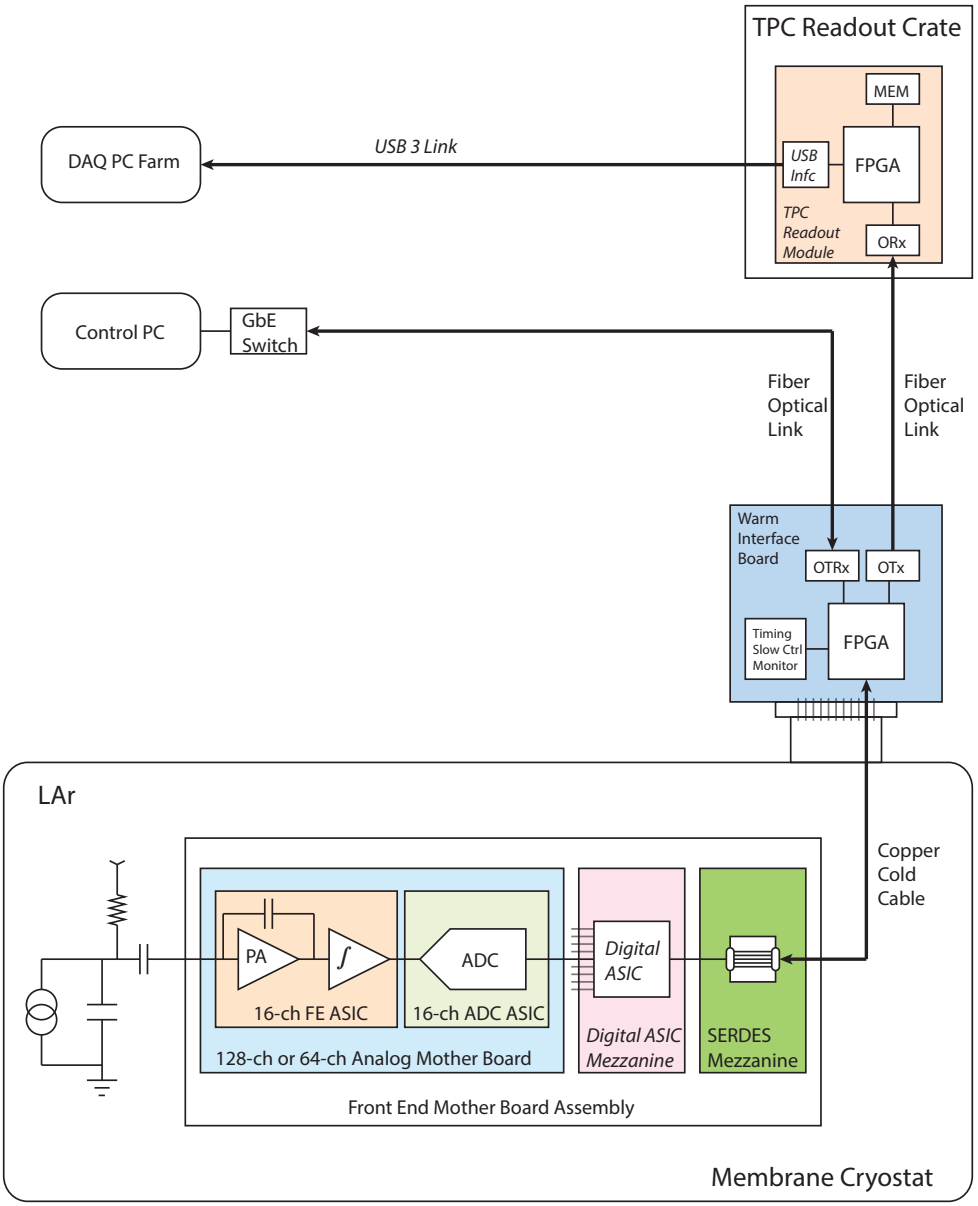

FIG. 22: *Information flow of a single TPC readout channel.*

of the particle momentum reconstruction based on track scattering angles. Deviations of the field map from perfectly uniform in a LAr-TPC may arise due to accumulation of positive argon ions in the drift volume. Ions are created by ionizing particles produced in neutrino interactions as well as by cosmic rays. While free electrons are quickly (within a few milliseconds) swept towards the readout system, ions have significantly lower mobility, and their drift velocity in a LAr detector at nominal drift field is of the order of 0.5 cm/s. The rate of cosmic muons in the fiducial volume of the LAr1-ND detector is estimated to be $\sim$2200 μ/s (or roughly 110 μ/m^2/s, considering only the top surface area). Positive ion charge is therefore produced by cosmic

ray muons at a rate of ∼1.7 nC/s. These ions are continuously neutralized at a cathode. An example of positive ion charge distribution in equilibrium for a LAr1-ND-like geometry is shown in figure 23, Left. Such accumulated volume charge leads to distortion of the drift field and, consequently, deviation of reconstructed track coordinates from the true ones by up to 2.5 cm (see figure 23, Right). Ion drift velocity is comparable to local argon flow velocities, produced by global argon re-circulation flow and thermal convection. Therefore, the resulting distribution of positive space charge inside the drift volume of the LAr1-ND TPC may show a sophisticated dynamic behavior.

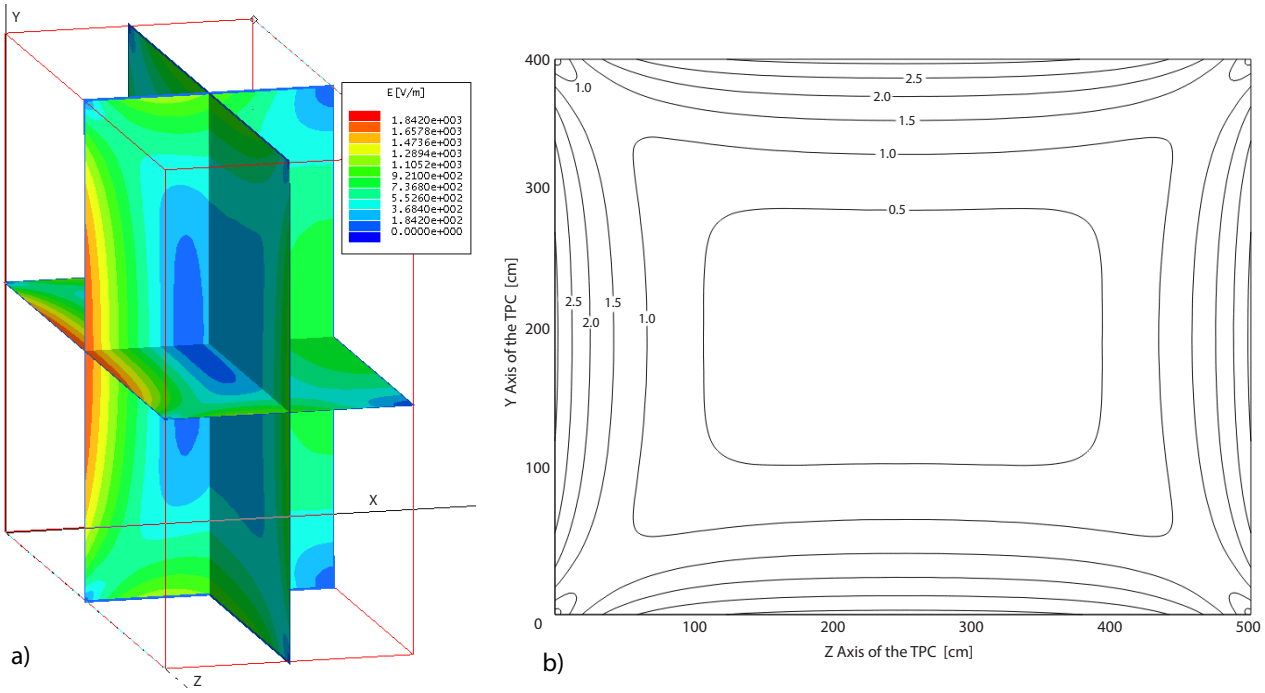

FIG. 23: *(Left) Electric field strength of the accumulated space charge on 3 orthogonal cut planes inside a drift volume of the one half of LAr1-ND (red outlined box). In this view the beam goes into the page (parallel to the z-xis), the cathode is on the left and anode is on the right. The nominal 500V/cm drift field is not included. This distorting field is high at the middle of the cathode, and middle of the wire planes, causing longitudinal distortions along the drift. The field is also relatively high at the middle of the field cage walls, causing transverse distortions. (Right) Maximum transverse distortion (lensing effect) in the TPC for electrons originating from the cathode surface. The magnitude of the distortion decreases when the electron starting point is closer to the wire planes.*

Analyzing the curvature of initially straight ionization tracks allows to reconstruct the distribution of the drift field vector across the whole volume of the detector [10]. This method was successfully exploited in the ARGONTUBE long drift TPC [11–13] to derive non-uniformity of the electric field along its 5 m long drift volume. The method to generate straight ionization tracks at defined locations in liquid argon is described in [14]. The thin photon beam from the pulsed UV laser with λ=266 nm ionizes argon via multi-photon absorption. The resulting ionization track is straight, characterized by low electron density, and therefore practically not subjected to charge recombination losses, unlike cosmic muon tracks. Those tracks are also free of δ-electrons, which complicate track reconstruction in the case of muons. For the MicroBooNE detector a set of such tracks are required in order to cover the whole sensitive

volume to reconstruct field distortion. Such tracks are created one-by-one by steering pulsed laser beams with the use of a custom-designed opto-mechanical feed-through (see [15]). The pulse rate of the laser generator is 10 Hz, capable of producing the minimum required set of 100 tracks within one minute (taking into account steering time).

B. Laser Beam Arrangement and Beam Optics

A typical scheme of producing a fan of straight ionization tracks from one laser source in a TPC is shown in Figure 24. A Nd:YAG laser (Surelite I-10) from Continuum, Inc. emitting light at a wavelength of 1024 nm is used as the primary light source. Inside the laser head nonlinear crystals are installed in the beam line for frequency doubling and summing, resulting in a wavelength of 266 nm, needed for ionization of liquid argon. The pulse maximum energy at this wavelength is 60 mJ and the pulse duration is ≈5 ns. The maximum repetition rate is 10 Hz. The beam has a divergence of 0.5 mrad and the diameter of about 5 mm.

The beam is delivered to the top of the rotating optical feed-through via a beam conditioning optics. This optics allows to set the beam attenuation and diameter and allows computer-controlled adjustment of the beam direction within few degrees. The feed-through brings the beam into the cryostat and provides a capability of steering it across the whole detector active volume. The arrangement of the four optical rotating units inthe LAr1-ND cryostat is shown in Figure 24, Right.

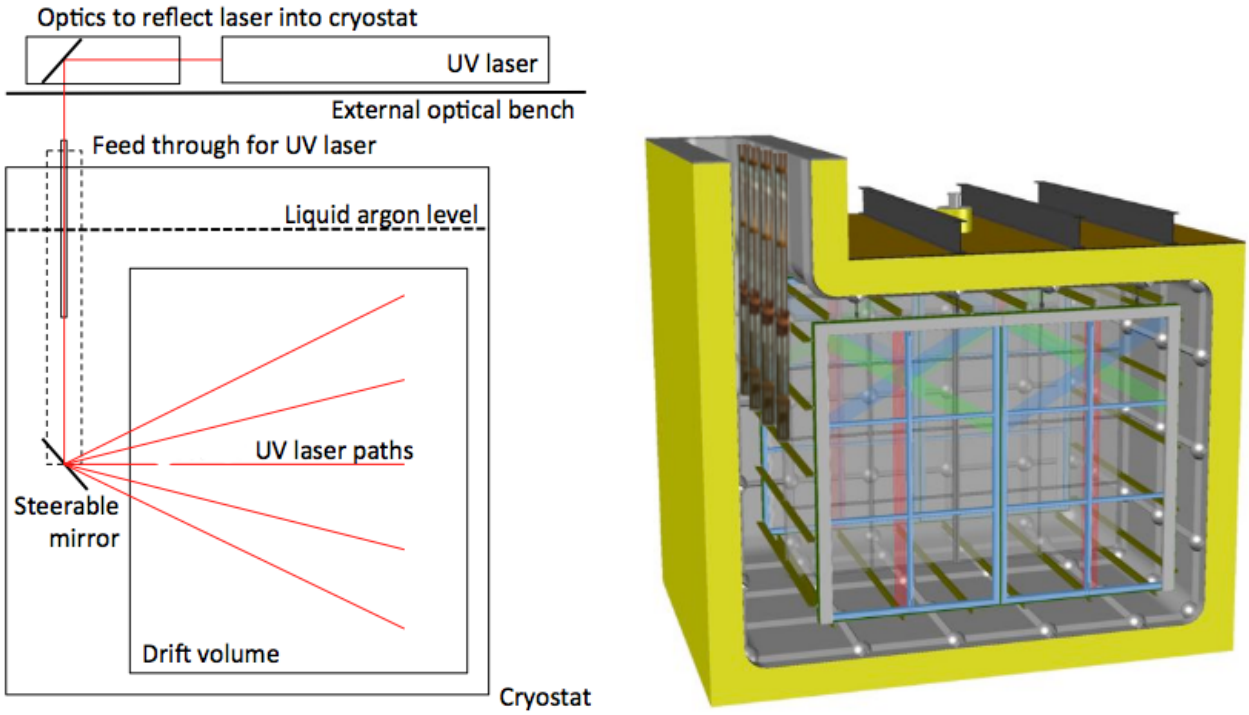

FIG. 24: *Left: a typical scheme of producing a fan of straight ionization tracks from one laser source in a TPC. Right: arrangement of four rotating optical feed-through in the LAr1-ND cryostat.*

The four steerable mirrors are located at half-height of the TPC active volume in front of corresponding beam entry apertures in the TPC field-shaping structure, as shown in Figure 26.

Each aperture has a diameter of 50 mm in order to maximize the deflection angle for the laser beam.

C. Rotating Feed-Through

To deliver undistorted UV laser beam into the active volume of the LAr1-ND detector, a rotating optical feed-through with the steerable mirror has been designed. The mirror is mounted on a horizontally rotatable support structure. A rack and pinion construction, where the mirror is mounted on the front side of a half gear (pinion) provides the necessary freedom for the vertical movement. All movable components are motorized to allow for remote control and automation of the mirror movement. The mirror support structure was fabricated out of polyamide-imide (Duratron T4301 PAI), which has a very low outgassing rate, low thermal expansion coefficient and is certified for operation at 87 K. To minimize the probability of discharges due to the close location of the feedthrough to the field cage, no conductive parts were used in the support structure. The two principal parts of the feedthrough are shown in Figure 25. At the left, the top rotating unit, operating at room temperature is seen. The steerable mirror, mounted at the bottom of the feedthrough support column, is shown at the right. In Figure 26 steerable mirrors mounted on the TPC field-shaping cage are shown. These units operates in liquid argon at the temperature of 87 K.

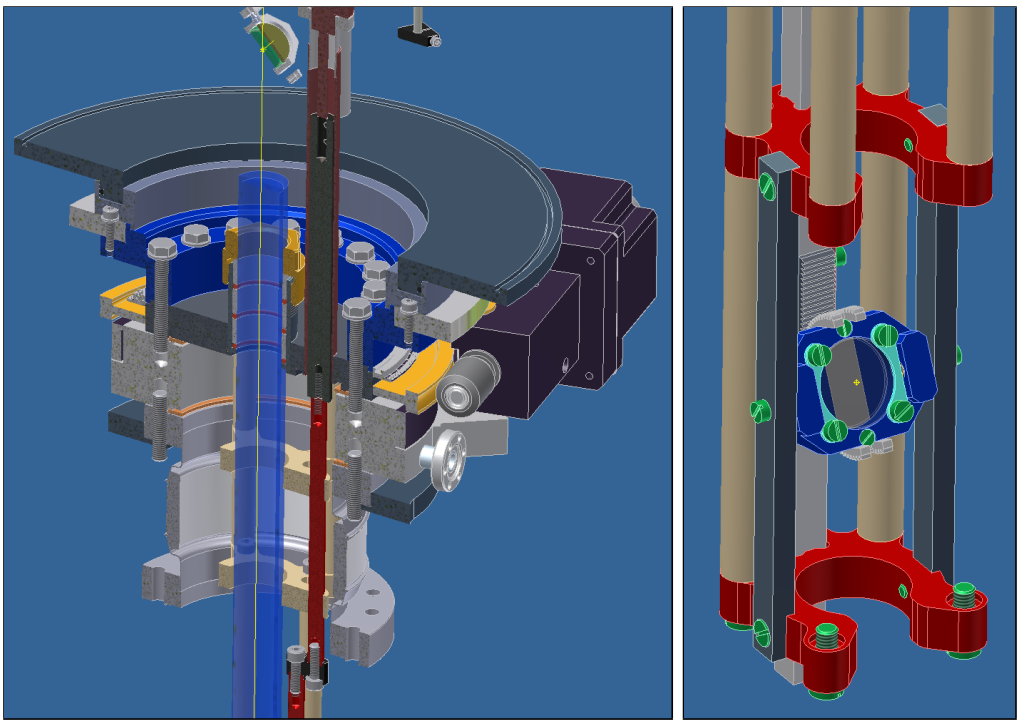

FIG. 25: *Left: CAD cutaway drawing of the feedthrough construction is shown. The yellow line indicates the path of the UV laser beam. Right: the cold mirror including the support structure.*

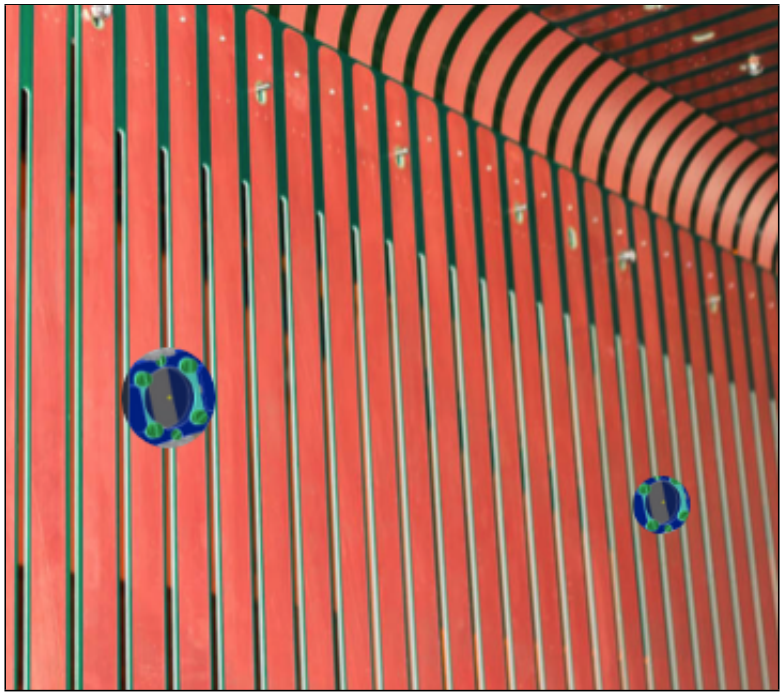

FIG. 26: *Steerable mirrors as seen through the 50 mm apertures in the TPC field-shaping cage.*

D. Expected Performance

An algorithm of field calibration has as input an array of detector events with one straight ionization track in each. The result of the algorithm is the coordinate correction map, which converts apparently curved track images back to true coordinate system, where they are straight. The algorithm is iterative with optimizable iteration step and therefore reconstruction accuracy. An example of simulated reconstruction in 2-D space is shown in Figure 27 for the case of a similar laser system that has been implemented in MicroBooNE. The distortion magnitude is reduced down to a few millimeters in 99% of the detector volume. A similar performance is anticipated for the LAr1-ND laser calibration system.

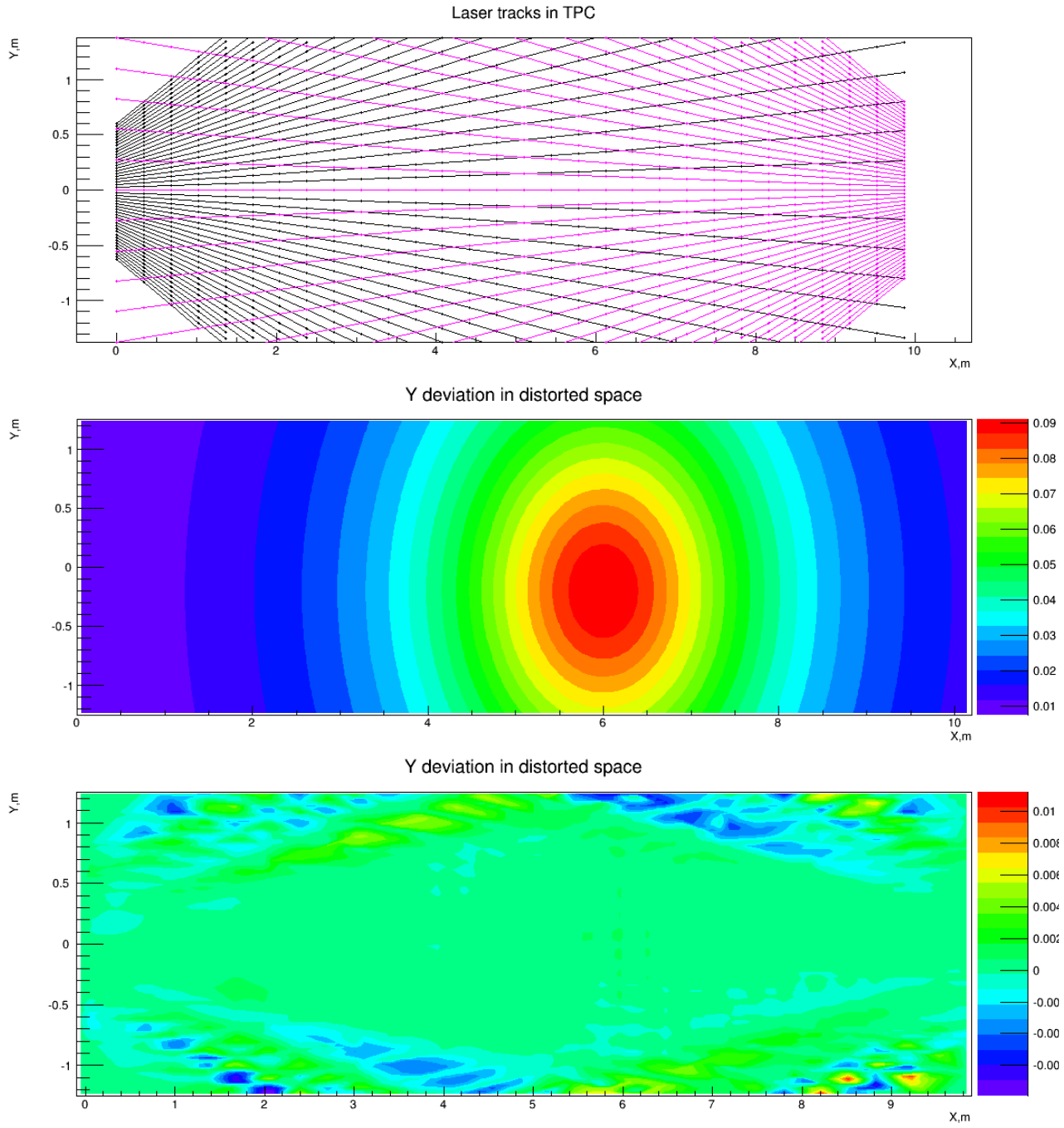

FIG. 27: *Example simulation based on MicroBooNE showing the performance of the laser calibration system. (Top) True laser beam trajectories in the MicroBooNE LAr-TPC. (Middle) map of Y coordinate of track deviation under influence of an ad-hoc non-uniform electric field, which in this example is slightly offset from center. (Bottom) map of the residual Y-coordinate deviation from the true ones after application of the reconstruction correction based on the laser tracks. The color scale in the lower two plots is in units of meters.*

VII. LIGHT DETECTION SYSTEM

A. Introduction and Motivation

Ionized and excited argon molecular states in the LAr volume will produce 128 nm vacuum ultraviolet (VUV) scintillation photons through recombination and de-excitation processes. The scintillation light includes a nanosecond-scale fast component (from singlet Ar_2^* decay with a lifetime ∼6 ns) as well as a microsecond-scale slow component (from triplet Ar_2^* decay with a lifetime ∼1.6 μs). Since recombination rates are reduced with higher electric field strength, a change in the field strength has opposite impacts on the amount of free ionization and scintillation light available for detection. At typical TPC field strengths, energy deposition by ionizing radiation is shared approximately equally between free ionization electrons and VUV scintillation photons, yielding approximately 2.9×10^4 e^-_{free}/MeV and 2.4×10^4 γ/MeV with a 500 V/cm electric field. It thus appears very appealing and natural to further optimize LAr-TPC detector performance by combining information from the available scintillation light with that from the ionization charge.

To be detected, scintillation photons are usually shifted from the vacuum ultraviolet to the visible to match the quantum efficiencies of available photodetectors, which typically peak around 430–450 nm. In most systems, this has been achieved using a fluorescent material to downshift the direct scintillation light (such as Tetraphenyl Butadiene, TPB) either coated on the surface of cryogenic photomultiplier tubes (as in ICARUS) or on plates mounted in front of the PMTs (as in MicroBooNE). PMTs must be located outside of electric field regions in the detector, thus in ICARUS and in MicroBooNE the PMTs are located just outside of the wire planes which are held close to ground. The resulting small photocathode area and limited solid angle coverage results in a relatively low light yield (∼1 phe/MeV for the past ICARUS system and ∼2 phe/MeV for MicroBooNE).

Detection of scintillation light can play several important roles in LAr-TPCs, depending on the time, energy, and position resolution performance of the light detection system (LDS) that is implemented. Increased collection efficiency could result in the improvement of all three performance metrics and enable improved background rejection and access to additional physics topics.

For a surface detector in a beam, prompt light signals provide a 'trigger', indicating when an interaction has occurred in coincidence with the neutrino beam. In LAr1-ND, neutrino interactions in the active TPC volume are expected in about 5% of the 1.6 μs long BNB beam spills. With a LDS time resolution of 1–2 ns, neutrino events could further be correlated with the 53 MHz Booster beam RF substructure (81 σ=1.15 ns wide pulses spaced 19 ns apart), leading to a potential 3-4× reduction in random cosmogenic backgrounds in the ν_e event sample (see Part I: Oscillation Physics Program). Figure 28 shows the BNB RF structure as measured by the MiniBooNE Cerenkov light detector. Also shown is the MiniBooNE time reconstruction of CCQE muon neutrino events relative to the beam RF time of the first proton pulse as determined by the Resistive Wall Monitor (RWM) discriminator. The CCQE muons exhibit the same time structure as the RF pulse, with a total time resolution of σ_t = 1.75 ns. The extra spread is due to RWM timing jitter and event reconstruction time resolution.

Good timing reconstruction resolution, in conjunction with the beam RF structure, can also be used to tag neutron events that are produced by neutrino interactions in the surrounding dirt. Due to the extended interaction geometry and subluminal speed of the neutrons, they interact in the detector out of phase with the beam RF time structure. This produces a flat time

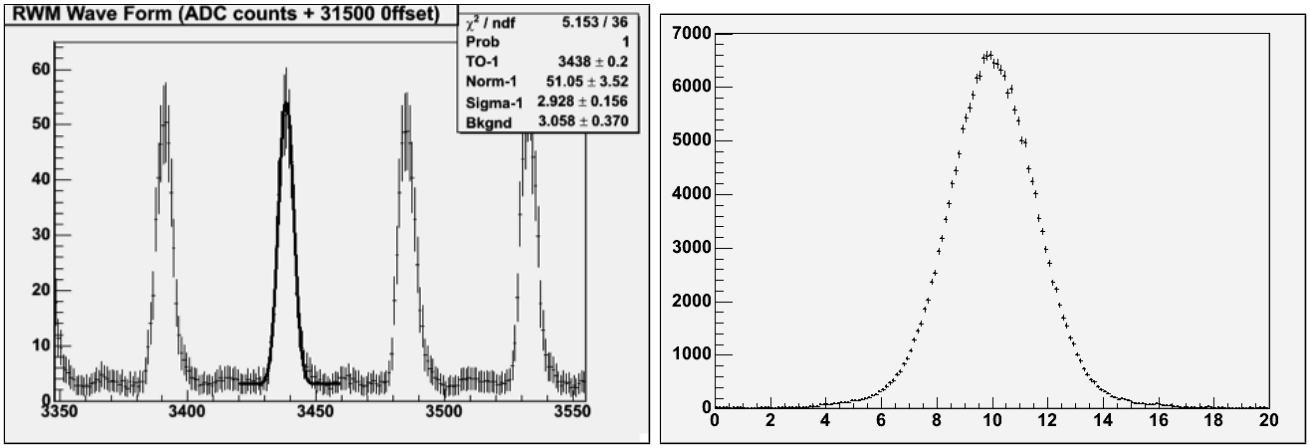

FIG. 28: *Left: The Booster-BNB 53MHz RF beam structure (2.5 counts/nsec). Right: the absolute time (nsec) reconstruction for CCQE muon neutrino candidates in MiniBooNE with all 81 bunches overlayed on top of each other, demonstrating that with good track timing, the RF structure of the beam can be reconstructed.*

response in the reconstructed bunch time (right plot of Figure 28), which can aid in background rejection and/or measurement of the neutron-dirt rate.

Prompt light signals also provide the unknown event t_0 necessary to reconstruct non-beam related events such as cosmic rays or supernova neutrinos. A system capable of associating multiple light pulses with their sources in the detector permits identification and 3D reconstruction of different events occurring throughout the 1.28 ms TPC readout window. The t_0 of each interaction in the detector is necessary to determine the location of the ionization along the drift direction and get an accurate reconstruction of the energy deposited along a track (by accounting for attenuation along the drift). The ability to identify the time of individual events will further contribute to rejecting cosmogenic backgrounds in the ν_e analysis. An average of 2.9 cosmic muons are expected in the TPC volume per readout window, distributed across the 20 m^2 area of the TPC (see Part I of this proposal). A position resolution of the LDS of better than 1 m would be needed to enable association of light signals with different activity in the detector. It should be noted, however, that the association with entering muons will be significantly aided by the external cosmic ray tagging system described in Section VIII B.

A LDS with increased detection efficiency could improve the reconstruction threshold of argon neutrino detectors to as low as a few MeV, enabling access to whole new fields of study such as low-energy nuclear effects. This requires a more uniform light collection as well as at least a ten-fold improvement in the collection efficiency compared to existing LAr neutrino detectors. In addition to lowering the threshold, using the scintillation light for calorimetric reconstruction allows the compensation of charge recombination effects, thereby increasing the linearity of the overall energy resolution in the detector. The improvement in resolution obtained by higher light collection has been demonstrated in simulation [16, 17] and an example of the power of such a combined energy calculation in xenon has been shown by the EXO collaboration [18].

An enhanced light readout system can also contribute to particle identification. The PID will derive from pulse shape discrimination (PSD) methods used in dark matter noble liquid detectors which effectively distinguish nuclear recoils from minimally ionizing particles (MIPs) using the time structure of the scintillation light alone. In neutrino interactions, this would aid in the separation of neutron interactions (which produce heavily ionizing recoil protons) from

gamma scatters (that produce minimally ionizing electrons).

Sufficient light collection may also provide a way of determining the sign of the incoming neutrino without using a magnetic field through improved tagging of Michel electrons coming from stopping muons, including those at lower energies. Efficient reconstruction of this very well known process is particularly helpful in argon because negatively-charged muons have a 75% capture rate on argon atoms, in which case there is no Michel electron emitted at the end of a muon track, whereas this capture does not happen for positively-charged muons. Ref. [17] shows that light detection systems with efficiency $\sim 1 \times 10^{-3}$ can isolate a sample of μ^- events with relatively little μ^+ contamination. This capability will be essential in raising the sensitivity in anti-neutrino running both in sterile neutrino searches and CP-violation searches in LBNF due to the large wrong-sign component of the anti-neutrino beam.

B. A Light Collection System for LAr1-ND

The relatively small volume of LAr1-ND makes it an excellent test-bed for new light detection system designs being considered for future LAr neutrino detectors, especially LBNF. The collaboration is committed to taking full advantage of this opportunity without incurring undue risk to the science goals of the SBN program. Hybrid systems that provide redundancy and side-by-side performance comparisons are also being considered and would fit well with the R&D goals of the experiment. LDS approaches currently being evaluated for LAr1-ND include: a system based on acrylic light guide bars read out at the ends with SiPMs, a system based on TPB-coated reflector foils to increase collection efficiency without increasing the number of photodetectors, and a traditional TPB-coated PMT based system.

Detailed MC simulations of the light generation and detection are being developed to compare reconstruction performance criteria such as track time, calorimetric energy, and position resolution. These results will inform the final design choice and determine the feasibility of a hybrid system comprised of elements from more than one of the present concepts. Studies are in progress and will be completed to enable a technology decision early in 2015.

1. Light Guide Bar Light Detection System

A light guide bar based light detection system has been initially proposed for LAr1-ND [5], based on a design originally developed for LBNE. In the LBNE design the system is positioned inside the APAs with wrapped wires. Thin profile light guides, measuring 100 cm × 2.54 cm × 0.64 cm, with wavelength shifter (WLS) deposited on their surface are used to collect the 128 nm LAr scintillation light. The WLS converts the VUV photons to ∼425 nm photons, some of which enter the bar. The downshifted photons are internally reflected to the end where they are detected by 3 SensL SiPMs whose QE is well matched to the ∼425 nm photons (See Fig. 29). This design allows one to collect light over a larger area with a relatively small number of readout channels. Four cast acrylic bars are assembled into "paddles". Each LBNE APA measures 7 m × 2.5 m and contains 20 of these light guide paddles. The solid angle subtended by an LBNE APA from a point displaced 2 m from its center is 15% and the fraction of the APA surface covered by light guides is 12%. A total of 108 APAs are used in each of 2 cryostats, totaling $108 \times 2 \times 20 \times 4 = 17,280$ light guide bars in LBNE.

The light guide photon detection system being considered for LAr1-ND aims to maximize the active area of the light guide bars to have both a high photon detection efficiency and

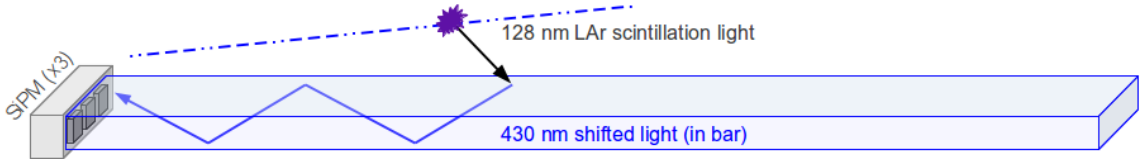

FIG. 29: *Cartoon of LAr scintillation light detection with a light guide coated with WLS.*

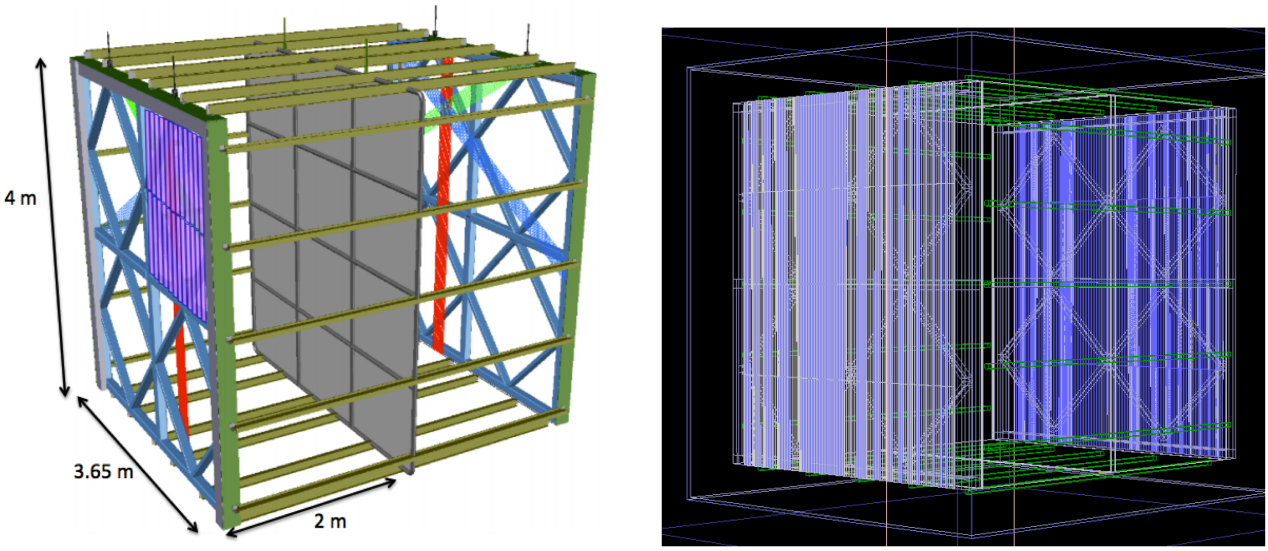

FIG. 30: ***Left:*** *Cartoon of the light guide design for LAr1-ND.* ***Right:*** *Light guide design implemented in Geant4.*

good granularity for timing and position resolution, which are especially valuable for a detector operating at the surface. The present design consists of 1,000 acrylic light guide bars coated with WLS embedded acrylic, each measuring 100 cm × 2.54 cm × 0.64 cm, mounted behind the LAr1-ND wire planes, as shown in Fig. 30. The solid angle subtended by a LAr1-ND APA from a point displaced 2 m from its center is 16% and the fraction of the APA surface covered by light guides is 87%. Both ends of each bar will be read out by an array of 3 SiPMs, smoothing out the position-dependent response of each bar and improving the overall light collection efficiency of each bar by a factor of ∼2 relative to the LBNE design. Furthermore, LAr1-ND will use new low-noise SensL SiPMs (MicroFC-60035-SMT), which have an order of magnitude lower dark rate.

The LAr1-ND light guide photon detection system builds off the LBNE design and therefore benefits directly from LBNE-related R&D efforts. Measurements of light guide bars in LAr have yielded valuable information on their performance and led to significant improvements in their design and quality. In particular, as an improvement over hand-painting the bars, the WLS solution is now applied to the surface by dip-coating the acrylic bars and then allowing them to dry in a low humidity environment. Recent measurements of these improved light guides have shown that attenuation lengths of over 100 cm are routinely achievable. Furthermore, preliminary data from studies of these light guides in pure LAr suggests that the global quantum efficiency (defined as the number of photoelectrons divided by the number of incident 128 nm photons) 50 cm from one end of the bar is ∼0.5%. Therefore, the global quantum efficiency when reading out both ends of the bar is expected to be $> 1\%$. Preliminary estimates indicate that

the light guide based photon detection system will collect 24 phe/MeV from a point displaced 2 m from its center and more than 24 phe/MeV when averaged over the entire TPC volume. A full MC simulation is in progress to confirm these performances.

2. TPB-coated Reflector Foil Light Detection System

A second design, based on a concept adapted from liquid argon dark matter detectors, proposes the installation of TPB-coated reflector foils inside the TPC volume to enhance light collection. The higher quantities of light collected would open the door to exploring physics topics not accessible to LAr-TPCs with standard readout schemes. By trapping light within the volume using TPB-coated reflective foils, light yield is enhanced naturally with less need to increase the number of DAQ readout channels as compared to solutions that achieve similarly-high light yields by scaling up photocathode coverage. A smaller number of readout channels allows for easier and more practical implementation of high-speed signal digitization, which would immediately improve the timing resolution of the system.

A system of this type is currently implemented in the LArIAT experiment (LAr-TPC In A Test Beam). LArIAT's light readout system collects many more scintillation photons than typical liquid argon neutrino experiments, with simulations estimating about 50 phe/MeV at zero field – substantially higher than the reach of both current and planned liquid argon neutrino detectors (∼1 phe/MeV for ICARUS, ∼2 phe/MeV for MicroBooNE, and ∼0.2-0.3 phe/MeV for the proposed LBNE system). The light yield simulation has been recently validated through measurements on a small-scale prototype where two high-QE cryogenic PMTs as well as three silicon photomultipliers (SiPMs) of different types were used to collect and read out scintillation light. Bench tests of the SiPMs mounted to custom on-board preamps are underway at FNAL and early results are encouraging. The forthcoming LArIAT test beam run will provide information both on technical and physical aspects of a reflective foil enhanced efficiency light system for LArTPCs.

The LArIAT optical system, with reflectors covering 60% of the active volume's inner surfaces and a photocathode coverage of about 0.5%, appears scalable up to the LAr1-ND dimensions with no need to transition through a dedicated R&D phase. A light collection efficiency enhanced to the level of 100 phe/MeV (corresponding to 0.5% photon detection efficiency) is the target light yield for the LAr1-ND design. A photocathode coverage of 1% coupled with 70% inner surface coverage of TPB-coated reflector foil is required to achieve this level [19]. For a LAr1-ND half-module, this translates to ∼750 cm^2 of distributed photocathode area and about 50 m^2 of TPB-coated foil covering the inner surfaces of the field cage and cathode. A full MC simulation is in progress to confirm these performances.

The wavelength-shifting TPB film (200 $\mu g/cm^2$) is deposited by vacuum evaporation on a substrate like Vikuiti ESR, a highly reflective and non-metallic foil made by multi-layer polymer technology. Each foil is 65 μm thick, and can be fashioned in a variety of different sizes (for example, 50× 50 cm^2) and mounted to thin, rigid supports with comparable coefficients of thermal expansion to create modular TPB-coated reflector tiles. These tiles can then be installed in an array to cover the inner surfaces of the field cage, and may also be easier to work with in the TPB deposition process.

The choice of photosensor is restricted to high-QE cryogenic PMTs, SiPMs, or a combination of the two. Adequate photocathodic coverage could be provided by 20 3-inch diameter PMTs positioned in an array behind the wire planes, or by 600 1.2 cm^2 SiPMs distributed behind the wire planes and possibly onto the field cage. Silicon photomultipliers offer several

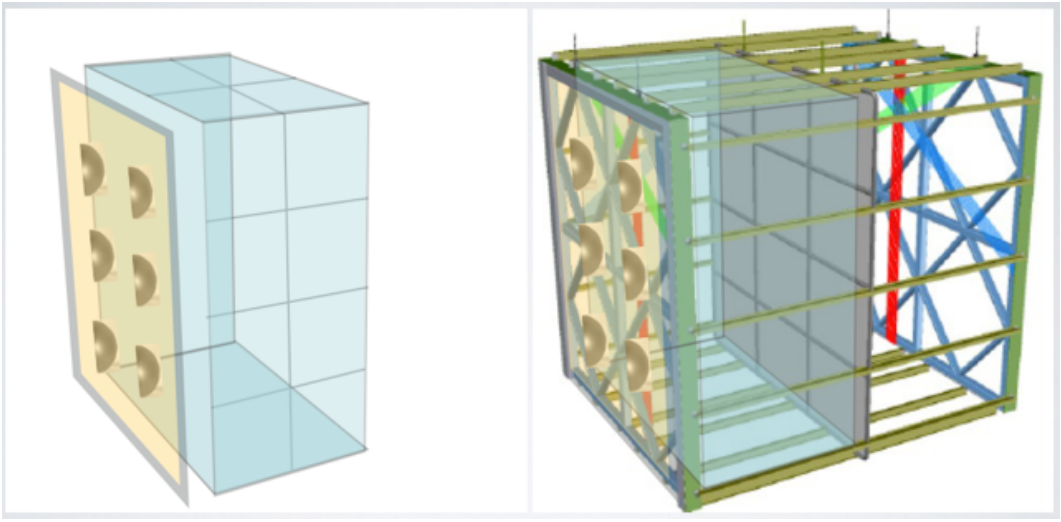

FIG. 31: *Schematic view of an enhanced efficiency light detection system in LAr1-ND. Shown on the left is the photosensor array behind the wire plane as well as modular TPB-coated reflector tiles lining the inner field cage of one half-module of the LAr1-ND detector.*

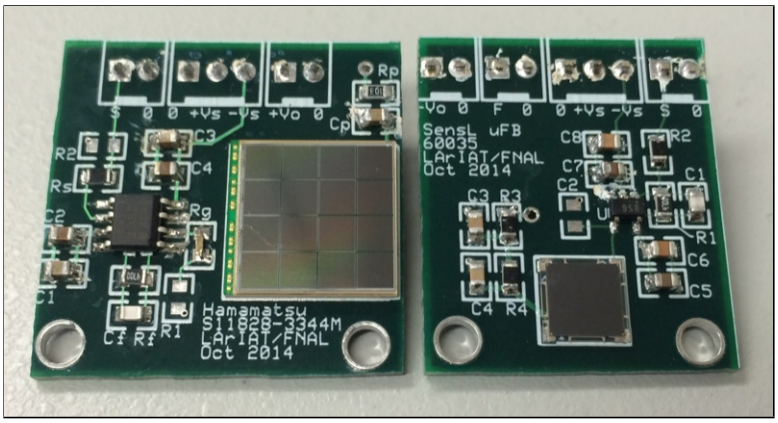

FIG. 32: *Custom readout electronics developed by LArIAT. Boards include bias voltage filtering, preamp, and readout for the Hamamatsu S11828-3344M, a 4x4 SiPM array with a total active area of* 1.2×1.2 *cm*^{2} *(left), and for the SensL MicroFB-60035 single SiPM channel with area* 0.6×0.6 *cm*^{2} *(right).*

notable advantages over PMTs, given their high QE coupled with small occupancy and low bias voltage. The forthcoming LArIAT run will provide full characterization of the SiPM response to LAr scintillation light in operating conditions to compare directly to PMT performance. Electronics for reading out SiPM arrays (groups of 16 SiPM channels combined in a single readout channel) as well as single channel SiPM chips, which include on-board bias voltage filtering and preamp/shaping circuitry as shown in Figure 32, have been developed. Further modifications to optimize the gain and timing response of the boards will be investigated. The TPB-coated reflector tiles described above may provide the necessary support for mounting variations of these miniature SiPM boards onto the field cage walls if such a layout proves advantageous.

The choice of the DAQ system for the TPB-coated reflector foil light detection system depends on the photosensor adopted, and in the case of PMTs, the limited number of readout

channels and the fast signal formation enables the use of fast waveform digitizers like the CAEN V1751 (10 bit, 1 GS/sec ADC) currently used in LArIAT. However, their use would require full and detailed engineering and augmented DAQ performance due to the potential increase in readout channels. The Silicon Photomultiplier signal Processor module described in Sect. VII B 4 seems an appropriate solution for the SiPM option, offering 14-bit, 150 MS/sec ADC for digitizing signals. This module have full waveform-recording capabilities with flash ADC, but also allows for flexible FPGA data processing algorithms needed for real-time pulse height and area measurements.

3. PMT-based Light Detection System

Light detection using TPB-coated cryogenic PMTs is known to work well in modest-sized LAr-TPCs, like the ICARUS T600 and MicroBooNE. This design is not easily scalable to big detectors, and different systems, like the ones reported in the previous sections, have been developed in view of larger LAr-TPCs for future applications.

In a PMT-based system, by using fast PMTs and good pixelization, the goal is to detect as much prompt and delayed scintillation light information (time and charge) as possible. This will then provide good event time and position reconstruction and track matching with the TPC. The preference is to have a transparent cathode to maximize the prompt light collection. A PMT-based system designed for LAr1-ND would use Hamamatsu R11065 3" diameter PMTs with 25% QE, and 6.5 ns transit time spread (full width at half max) at LAr temperatures. The PMTs are flat face and would have a 3" TPB wavelength shifter affixed to the surface. The combined PMT+TPB efficiency at 128 nm is expected to be 12.5% .

The LAr1-ND detector instrumented with 121 PMTs on each side arranged in an 11×11 grid over a $4\ m \times 4\ m$ frame would have 1% total photocathode coverage, or 6.7% on each of the instrumented sides. Light yield in this configuration is estimated to be 13 phe/MeV for a source 2 m away from the the center of an APA, where about 25% (50%) comes as prompt light for lightly (heavily) ionizing particles. A full MC simulation is in progress to confirm these performances. The option to instrument the outer veto region (LAr outside the active TPc boundaries) is being investigated as well.

4. Electronics for the Light Detection System

Several options exist for reading out SiPM or PMT signals, each of which has its own relative merits. These options include a direct signal digitization or the signal digitization after SiPM/PMT pulse shaping. Fast (direct) digitization of SiPM pulses has been implemented by the HEP Electronics Group at Argonne National Laboratory (ANL) to support the development of the photon detection systems for LBNE. The FEE developed at ANL is being adopted for SiPM readout, but the implementation is flexible and may be modified for use with PMTs, if desired.

Each SSP (SiPM Signal Processor) module (Fig. 33) consists of 12 readout channels packaged in a self-contained 1U module. Each channel contains a fully-differential voltage amplifier and a 14-bit, 150 MSPS analog-to-digital converter (ADC) that digitizes the waveforms received from the SiPMs. The digitized data is then processed by a Xilinx Artix-7 Field-Programmable Gate Array (FPGA). The FPGA implements an independent Data Processor (DP) for each channel. The processing incorporates a leading edge discriminator for detecting events and a

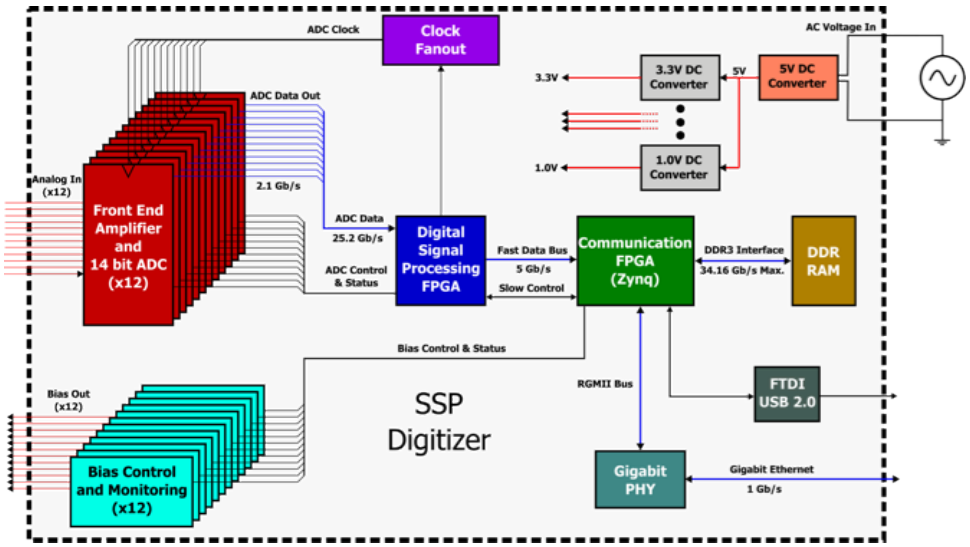

FIG. 33: *Block diagram and physical realization of the prototype SSP module.*

constant fraction discriminator (CFD) for sub clock timing resolution. In the simplest mode of operation, the module can perform waveform capture, using either an internal trigger or an external trigger. As an alternative to reading full waveforms, the Data Processors can be configured to perform a wide variety of data processing algorithms, including several techniques for measuring amplitude, and also timing of the event with respect to a reference clock.

If a faster timing response becomes one of the requirements of the photon detection system, a faster ADC with a shaper will be incorporated into the front-end electronics to achieve improved timing resolution. The present system samples the waveforms at 150 MSPS, and achieves ∼2-3 ns resolution on single photo-electron signals. Given that the time constant of the prompt light is 6-7 ns, it may become necessary to improve the timing resolution to the sub-nanosecond level. This would require the use of faster ADCs and possibly pulse shaping. This is not part of the system specifications currently, but would be an R&D activity should the performance be required.

VIII. COSMIC RAY TAGGING SYSTEM

As described in Part I of this Proposal, cosmic ray muons are the most abundant background in a LAr-TPC at surface. Although muons do not contribute significantly to the background for the sterile neutrino search, they produce δ-rays, which in turn produce photons by Bremsstrahlung. These photons, via Compton scattering or pair production, could possibly mimic a ν_e-like interaction signature.

The addition of a cosmic ray tagging system, that detects cosmic ray muons and measures their time and position relative to events internal to the TPC, is a way to mitigate the cosmic ray background.

From Monte Carlo simulations, the average number of cosmic muon tracks, seen in each of the LAr1-ND TPC events is about 3. Each muon track is surrounded by tracks of electrons and positrons, originating from Bremsstrahlung of delta-electrons produced by muons, and, for rare very high energy muons, by muon Bremsstrahlung in the liquid argon. The cosmic ray tracker system chosen for the LAr1-ND detector is composed of scintillators external to the LAr1-ND

cryostat providing 4π solid angle coverage.

A. Scintillating Tracker Design and Operation

The LAr1-ND cosmic ray tracker is composed of scintillating planes, each consisting of an array of 1x10x400 cm scintillating bars as shown in Figure 34. One plane provides coordinate resolution in X - and the adjacent plane provides resolution in Y coordinate. In the following description each such sandwich is referred to as X-Y tracker plane.

Each bar is made of BC-440 (or similar) plastic scintillator with the emission maximum at 434 nm and bulk attenuation length of >400 cm. The bar is wrapped in a diffuse reflector foil (Tyvek) to make the light field inside the bar more uniform and, additionally, in an aluminum-coated Mylar foil. The insensitive gap between two adjacent bars is about 0.5 mm.

In order to provide a more efficient and uniform collection of scintillation light along the bar, two wavelength-shifting fibers (1 mm diameter multi-clad Kuraray WLS Y11(200) S-type [20]) are glued into the scintillating bar near its edges at both lateral sides. The light is transmitted by the fibers to the bar edge, where it is detected by the Hamamatsu S12825-050P multi-pixel Geiger avalanche photo-diodes (MAPDs, also known as SiPMs). Matching of the Y-11 emission spectrum to the SiPM sensitivity is illustrated in Figure 35.

In order to mitigate cosmic ray events, a 4π solid angle coverage of the TPC is highly desirable. On the top, where the flux of cosmic rays is maximum, an additional X-Y plane is installed at the distance of 2 m above the X-Y plane covering the top surface of the TPC as shown in Figure 36. These two planes in combination form a telescope, that provides coordinate resolution of $10/\sqrt{12} \approx 2.9$ cm at the detector planes and angular resolution of $2 \times 2.9/200 \approx 0.03$ rad.

In order to increase the rejection of the EM background and the detection efficiency of ν_e CC interactions the following algorithm is proposed. The time distribution of the muon-related signal from the scintillating tracker is compared to that of the internal TPC light detection system and to the beam gate. Muon tracks, detected in the TPC are extrapolated to the scintillating planes. The time distribution of the signal from the scintillating tracker channels, that are crossed by the extrapolated muon trajectories is used to build correspondence with the internal TPC light collection system signals. Those tracks, that are seen by the tracker and internal light collection system outside of the beam gate are unambiguously identified as cosmic muons, The remaining event with the signature of no signal in scintillating tracker and the signal in the TPC light collection system in time with the beam gate can be identified as the beam-related. All 7 X-Y planes of the scintillating tracker are essential for this procedure.

B. Electronic Readout System

As mentioned above, in the proposed design the Hamamatsu S12825-050P photodiodes are used to convert wavelength-shifted scintillation light to the electronic analog signal. The most relevant parameters of these diodes are shown in Figure 37 as a function of the over-voltage (the difference between the applied reverse-bias voltage and the breakdown voltage). At the over-voltage of 2.0 V the PDE at the maximum of the spectral sensitivity is about 32% and the gain exceeds 10^6. The pulse frequency at the threshold allowing to detect single photons is of the order of 100 kHz at 20°C. The signal from photodiode is amplified and shaped by a CITIROC multi-channel front-end ASIC, designed by Omega. The analog signals are discriminated at

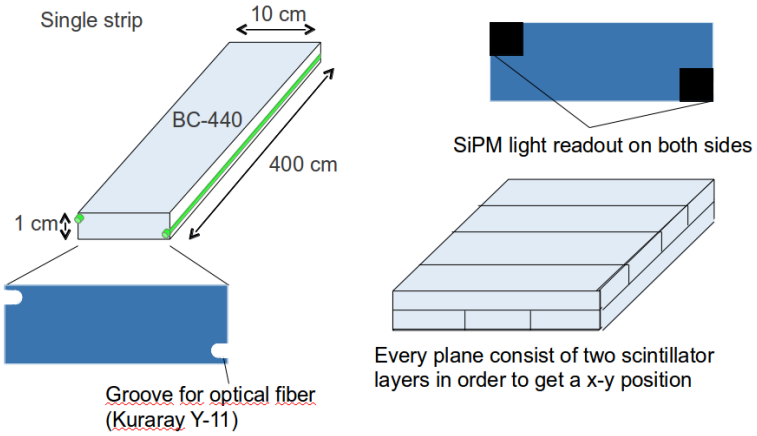

FIG. 34: *Veto plane composition: scintillating bars with WLS fibers glued into grooves along strip sides. The material for the bars is BC-440 or similar plastic scintillator. Scintillation light is collected with Kuraray Y-11 WLS fibers and transmitted to the bar edge, where it is detected by Hamamatsu S12825-050P SiPMs.*

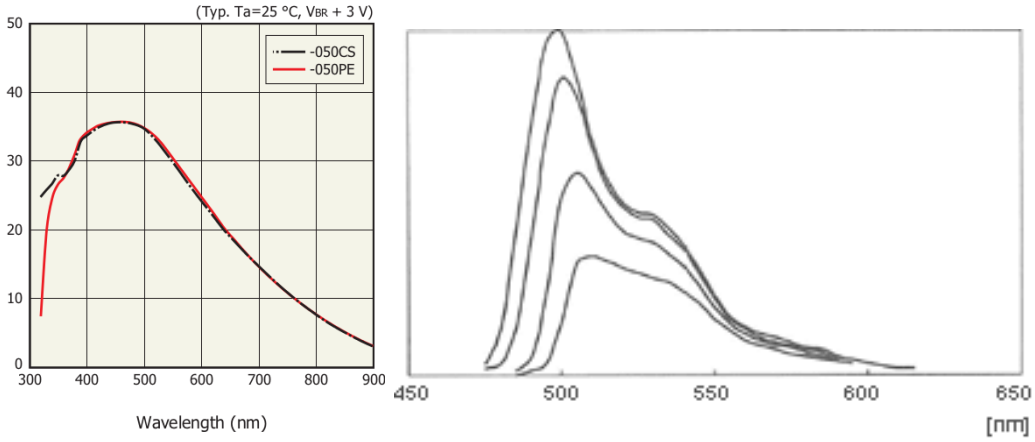

FIG. 35: *SiPM spectral sensitivity (left), and emission spectrum from Y11 WLS fiber (right).*

the level of a 1.5 of single photo-electron response. To suppress the dark current rate the logic coincidence is used at each end of the scintillating bar, between the signal from two diodes glued to two WLS fibers at each side of the bar. The resulting logic signals together with digitized peak values of the shaped analog signals and time stamp are stored in a FIFO buffer and eventually transmitted via Ethernet link to the experiment DAQ system for event building and storage.

C. Expected Performance

The performance of the proposed tracker configuration is estimated on the base of the experimental data published in reference [21]. The authors studied the light yield and timing characteristics of a similar scintillating tracker with 16 m long scintillator bars, Kuraray Y-11(200)S WLS fiber and Hamamatsu S10362-13-050C photodiodes, very similar to S12825-050P used in the present proposal. The thickness of the bars studied was 7 mm and the width from

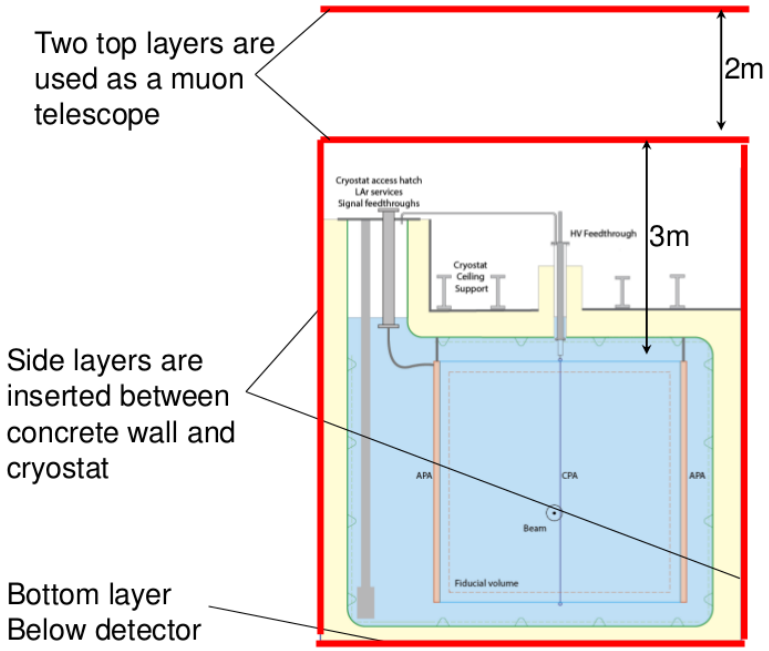

FIG. 36: *Veto planes arrangement around the detector.*

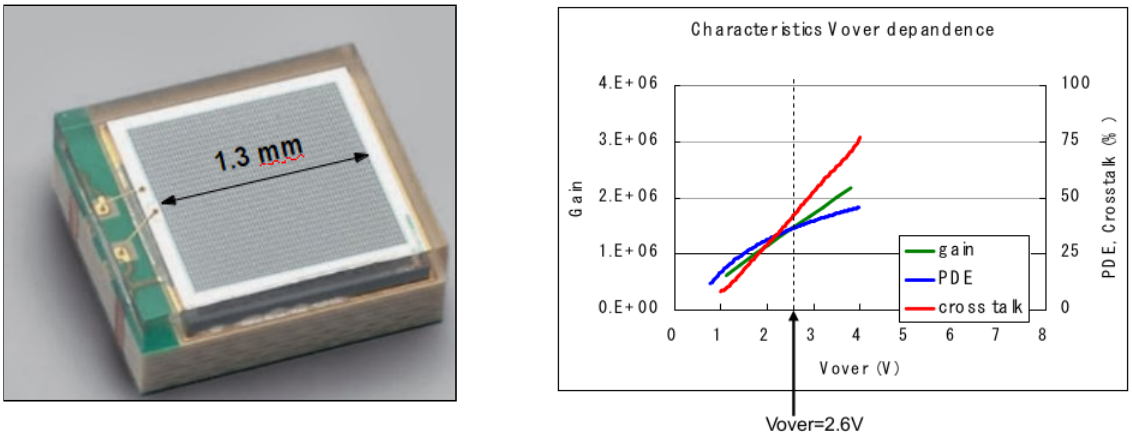

FIG. 37: *Hamamatsu S12825-050P SiPM (left), photon detection efficiency (PDE), noise and pixel cross-talk as a function of over-voltage at 408 nm (right).*

1 cm to 4 cm. The effective attenuation length was found to be ≈ 4.2 m. Extrapolating their data to the case of 1x10x400 cm bars yields the expected data on light yield, shown in the table IV. The detection inefficiency in each channel is calculated as a Poisson probability to obtain a signal lower than 2 p.e. The single end trigger inefficiency is given by the logic AND between left and right channels at each end of the bar.

The velocity of the re-emitted light propagation in the Y11 fiber is found to be 16.00±0.08 cm/ns and the decay time of Y11 fiber 12±0.5 ns [21]. Therefore the coincidence window for left and right discriminated signals is conservatively chosen to be about 100 ns (defined by CITIROC FE ASIC timing characteristics). The rate of dark current pulses above the 1.5 p.e. threshold is about 10 times lower than that for single photo-electron [22], that is of the order of 10 kHz. The resulting rate of accidental left-right coincidence is about 10 Hz. Such a low

TABLE IV: *The summary on the expected MIP light yield and detection efficiency for the proposed cosmic ray tracker. The data is obtained by extrapolation of experimental results published in [21].*

	Near end (1.0 m)	Far end (4.0 m)
Light yield, p.e.	22	11
Detection inefficiency	$6.4\text{x}10^{-9}$	$2.0\text{x}10^{-4}$
Single end trigger inefficiency	$1.2\text{x}10^{-8}$	$4.0\text{x}10^{-4}$
Single channel dark count rate	10 kHz	10 kHz
Single end trigger dark count rate	10 Hz	10 Hz

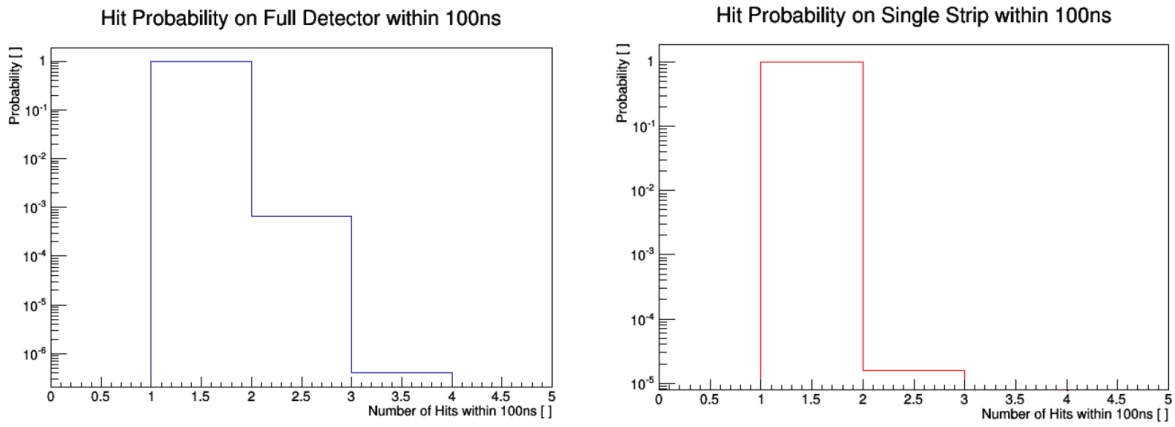

FIG. 38: *The expected muon multiplicity over the whole top scintillator plane (left) and over one 1x10x400 cm scintillator bar.*

rate allows us to minimize the useless part of the data flow from the scintillating tracker and to use inexpensive low-rate transmission channels from the tracker planes to the processing unit. At the processing unit a more sophisticated logic of correlation of the signals from both ends of the bar, as well as with the signals from the perpendicular bars can be implemented.

The expected minimum sum of the signal from both ends of the bar is 36 p.e. on each of the left and right WLS fiber channels. The total sum per bar is therefore 72 p.e. The minimum total sum of the dark count pulses is 2x4=8 p.e. Setting a constraint of having the total sum per bar of at least 20 p.e will bring the rate of fake hits per bar down by more that ten orders of magnitude, making it negligible. The additional inefficiency introduced by such cut is of the order of 10^{-13}, therefore, also negligible.

The probability of the multiple muons hitting the same scintillator channel is estimated from the Monte-Carlo simulation of cosmic muon flux at the detector surface by CRY simulation package. The resulting multiplicities are shown in Figure 38. The graph at the left shows average multiplicity of muon tracks in the whole top 4x4 m^2 surface of the tracker X-Y plane, while the right plot shows the multiplicity in each single scintillating bar within 100 ns of the signal integration period. The probability to have more than one hit per bar is of the order of 10^{-5}.

Since the detection inefficiency of the proposed light readout system is negligible, the total detection efficiency of the tracker is limited by the 0.5 mm thick insensitive gaps between adjacent scintillating bars. The detection efficiency of one coordinate plane is therefore about 99.5%. If the coincidence of X and Y planes is required, the detection efficiency drops to 99% per X-Y plane.

IX. THE LAR1-ND DETECTOR: A DEVELOPMENT TOWARD LBNF

LAr1-ND presents an excellent opportunity for the continued development of the LAr-TPC technology toward the LBNF program. The design of the LAr1-ND detector is largely based on current LBNF-type technology, but alternate solutions can also be pursued where it is valuable to inform final choices for the LBNF detector. The designers of LAr1-ND systems are, in many cases (i.e. cryostat, cryogenics, TPC, cold electronics), the same teams working on LBNF designs, ensuring good communication of ideas and lessons learned. LAr1-ND's location 110 m from the Booster Neutrino Beam target will provide a unique opportunity to test specific components and new concepts in a high-rate neutrino beam.

Tables V, VI, and VII compare different systems of the LAr1-ND and LBNF detector designs, highlighting key similarities and differences.

A comparison of the LAr1-ND and LBNF design of the cryostat and cryogenic systems is reported in Table V. The same membrane-style cryostat is used. One difference is the location of the cryogenic pumps. Also, in LAr1-ND, there is the possibility that the liquid completely fills the main volume, touching the top plate, in order to minimize the outgassing from the surface and cabling. This choice is currently under study.

Table VI compares the features of the LAr1-ND and LBNF TPC designs and many similarities exist. The main difference is that the LAr1-ND design does not wrap the readout wires around the APA frames since this is not needed with the drift volume only on one side.

As reported in Table VII the LAr1-ND electronics is largely based on an already developed LBNF design. The choice of the cold FPGA for digital processing is due to the long lead time needed to develop a dedicated ASIC for this task. This work is underway, and could be tested in the detector in a future phase of running.

Finally, as discussed in Section VII, LAr1-ND provides an excellent test-bed for light collection systems in a LAr detector. The TPB coated acrylic light guide design is based on concepts developed for LBNF, and LAr1-ND will be a direct test of this approach in a running neutrino experiment. Other approaches are being developed in attempt to enhance light collection with increased collection efficiency and improved time resolution. LAr1-ND provides an opportunity to test new approaches, possibly side-by-side, with the goal of informing an optimized design for LBNF in the future.

Cryostat/ Cryogenics	LAr1-ND	LBNF	Comparison
Cryostat Technology	Membrane	Membrane	Same commercial technology using passive foam insulation
LAr pump	Outside cryostat	Inside cryostat	Test alternate concept
Ullage space	In the cryostat OR confined to a region over inactive region	In the cryostat	Isolated expansion region being considered; allows the main cryostat to be completely filled with LAr, reducing outgassing from warm surfaces inside the cryostat
Purification	Dual phase during filling, gas phase thereafter	Dual phase throughout	With the warm ullage in a separate area in LAr1-ND, a much smaller scale purification system can be used in the small gas volume during the normal operation of the TPC

TABLE V

TPC	LAr1-ND	LBNF	Comparison
Construction	Pre-fabricated/tested modules assembled in cryostat or on-site	Pre-fabricated/tested modules assembled in cryostat	Same concept, different implementation
TPC Support	Suspended under cryostat roof	Suspended under cryostat roof	Same concept, different implementation
TPC configuration	CPA in the middle, single sided APAs against the walls	CPAs against the walls, double sided APAs in the middle	Avoid a costly fiducial cut around the non-active thickness of the APA in the center of the active region. The APAs can be placed closer to the cryostat walls to maximize active region in the limited available space.
APA configuration	Single sided, no helical wire wrapping, readout on 3 edges	Double sided, helical wire wrapping on two induction planes, readout on one edge	LAr1-ND's APA design avoids the wire wrapping, while allowing APA tiling on all 4 sides. Learn from LBNF 35 ton TPC prototype. The LAr1-ND design provides a verified alternative to the LBNE APAs.
APA wire configuration	3 sense wire planes, +/- 60 degree, 3mm wire pitch, identical to MicroBooNE	3 sense wire planes, +/- 45 degrees, 4.5-5mm wire pitch	LAr1-ND's wire configuration is identical to MicroBooNE
APA wire bonding	CuBe wires epoxyed and soldeded to PCB with notched edges	CuBe wires epoxyed and soldeded to PCB with notched edges	Same design
CPA design	Stainless steel frame + conductive sheet	Stainless steel frame + conductive sheet	Same design concept, light transmission TBD
Field cage design	Cu strips on FR4 panels	Cu strips on FR4 panels	Similar design

TABLE VI

Electronics	LAr1-ND	LBNF	Comparison
Analog Front-End	ASIC	ASIC	Same design
ADC	ASIC	ASIC	Same design
FE Digital Processing	FPGA	FPGA or ASIC	LAr1-ND will use FPGA to meet fast schedule
Front End Board	Analog Mother Board + Digital Mezzanine	Analog Mother Board + Digital Mezzanine	Similar design, different mechanical dimension and channel density
Cold Cable	Twinaxial Cable	Twinaxial Cable	Same design
Signal Feed-through	ATLAS Pin Carrier	Flange Board or ATLAS Pin Carrier	LAr1-ND will use already developed technology ATLAS pin carrier.
Warm Interface Board	FPGA + Optical Transceiver	Optical Transceiver and/or FPGA	LAr1-ND will use FPGA to study data compression and trigger algorithm, and keep the capability to stream all data out
Data Concentrator Board	Commercial PCIe Card	SLAC RCE	LAr1-ND will use commodity hardware in DAQ system, focus efforts on algorithm, firmware and software development

TABLE VII

[1] A.A. Aguilar-Arevalo *et al.* (MiniBooNE Collaboration), "A Search for Electron Antineutrino Appearance at the $\Delta m^2 \sim 1$ eV^2 Scale," Phys.Rev.Lett. **103**, 111801 (2009), arXiv:0904.1958 [hep-ex].

[2] H. Chen *et al.* (MicroBooNE Collaboration), "Proposal for a New Experiment Using the Booster and NuMI Neutrino Beamlines: MicroBooNE," (2007).

[3] D. Kaleko, "Low Energy Excess: MiniBooNE to MicroBooNE," MicroBooNE Document 3862 (2014).

[4] A.A. Aguilar-Arevalo *et al.* (MiniBooNE Collaboration), "Event Excess in the MiniBooNE Search for $\bar{\nu}_\mu \to \bar{\nu}_e$ Oscillations," Phys.Rev.Lett. **105**, 181801 (2010), arXiv:1007.1150 [hep-ex].

[5] C. Adams *et al.*, "LAr1-ND: Testing Neutrino Anomalies with Multiple LAr TPC Detectors at Fermilab," (2014), FERMILAB-PROPOSAL-1053.

[6] P. Wilson *et al.*, "Program Definition Status Report: Short-Baseline Neutrino Oscillation Program on the Fermilab Booster Neutrino Beam," submitted to the Fermilab PAC in July 2014.

[7] A. Blatter, A. Ereditato, C C. Hsu, S. Janos, I. Kreslo, M. Luethi, C. Rudolf von Rohr, M. Schenk, T. Strauss, M S. Weber, and M. Zeller, "Experimental study of electric breakdowns in liquid argon at centimeter scale," JINST **9**, P04006 (2014).

[8] J. Asaadi, J M. Conrad, S. Gollapinni, B J P. Jones, H. Jostlein, J M. St John, T. Strauss, S. Wolbers, and J. Zennamo, "Testing of high voltage surge protection devices for use in liquid argon TPC detectorss," JINST **9**, P09002 (2014).

[9] D. Axen, R. Hackenburg, A. Hoffmann, S. Kane, D. Lissauer, D. Makowiecki, T. Muller, D. Pate, V. Radeka, D. Rahm, M. Rehak, S. Rescia, K. Sexton, J. Sondericker, P. Birney, A. W. Dowling, M. Fincke-Keeler, T. Hodges, F. Holness, N. Honkanen, R. Keeler, R. Langstaff, M. Lenckowski, M. Lefebvre, P. Poffenberger, G. Vowles, and C. Oram, "Signal feedthroughs for the atlas barrel and endcap calorimeters," Review of Scientific Instruments **76**, 063306 (2005).

[10] A. Ereditato, D. Goeldi, S. Janos, I. Kreslo, M. Luethi, *et al.*, "Measurement of the drift field in the ARGONTUBE LAr TPC with 266 nm pulsed laser beams," (2014), arXiv:1408.6635 [physics.ins-det].

[11] I. Badhrees, A. Ereditato, S. Janos, S. Haug, I. Kreslo, *et al.*, "Argontube: An & liquid Argon Time Projection Chamber," JINST **7**, C02011 (2012).

[12] A. Ereditato, C.C. Hsu, S. Janos, I. Kreslo, M. Messina, *et al.*, "Design and operation of ARGONTUBE: a 5 m long drift liquid argon TPC," JINST **8**, P07002 (2013), arXiv:1304.6961 [physics.ins-det].

[13] M. Zeller, A. Ereditato, S. Haug, C.C. Hsu, S. Janos, *et al.*, "First measurements with ARGONTUBE, a 5m long drift Liquid Argon TPC," Nucl.Instrum.Meth. **A718**, 454–458 (2013).

[14] I. Badhrees, A. Ereditato, I. Kreslo, M. Messina, U. Moser, *et al.*, "Measurement of the two-photon absorption cross-section of liquid argon with a time projection chamber," New J.Phys. **12**, 113024 (2010), arXiv:1011.6001 [physics.ins-det].

[15] A. Ereditato, R. Hnni, I. Kreslo, M. Lthi, C. Rudolf von Rohr, *et al.*, "A steerable UV laser system for the calibration of liquid argon time projection chambers," (2014), arXiv:1406.6400 [physics.ins-det].

[16] M. Szydagis, "NEST (Noble Element Simulation Technique)," FNAL, Software Workshop, 2013.

[17] M. Sorel, "Expected performance of an ideal liquid argon neutrino detector with enhanced sensitivity to scintillation light," JINST **9**, P10002 (2014), arXiv:1405.0848 [physics.ins-det].

[18] J. B. Albert *et al.* ((EXO-200 Collaboration)), "Search for Majoron-emitting modes of double-beta

decay of ^{136}Xe with EXO-200," Phys. Rev. D **90**, 092004 (2014).
[19] E. Segreto, "An analytic technique for the estimation of the light yield of a scintillation detector," JINST **7**, P05008 (2012), arXiv:1100.6370 [physics.ins-det].
[20] Kuraray Co, Methacrylic Resin Division, Tokyo, Japan,.
[21] O. Mineev, Yu. Kudenko, Yu. Musienko, I. Polyansky, and N. Yershov, "Scintillator detectors with long WLS fibers and multi-pixel photodiodes," JINST **6**, P12004 (2011), arXiv:1110.2651 [physics.ins-det].
[22] Hamamatsu Photonics, "MPPC Technical Information," http://www.hamamatsu.com/resources/pdf/ssd/mppc_techinfo_e.pdf.